NEUROSCIENCE

Polygenic risk for alcohol use disorder affects cellular responses to ethanol exposure in a human microglial cell model

Xindi Li[1], Jiayi Liu[2,3], Andrew J. Boreland[1], Sneha Kapadia[1], Siwei Zhang[4,5], Alessandro C. Stillitano[1], Yara Abbo[1], Lorraine Clark[1], Dongbing Lai[6], Yunlong Liu[6], Peter B. Barr[7], Jacquelyn L. Meyers[7], Chella Kamarajan[7], Weipeng Kuang[7], Arpana Agrawal[8], Paul A. Slesinger[9], Danielle Dick[10], Jessica Salvatore[10], Jay Tischfield[11,12], Jubao Duan[4,5], Howard J. Edenberg[6], Anat Kreimer[2,3], Ronald P. Hart[11,13], Zhiping P. Pang[1]*

Polygenic risk scores (PRSs) assess genetic susceptibility to alcohol use disorder (AUD), yet their molecular implications remain underexplored. Neuroimmune interactions, particularly in microglia, are recognized as notable contributors to AUD pathophysiology. We investigated the interplay between AUD PRS and ethanol in human microglia derived from iPSCs from individuals with AUD high-PRS (diagnosed with AUD) or low-PRS (unaffected). Ethanol exposure induced elevated CD68 expression and morphological changes in microglia, with differential responses between high-PRS and low-PRS microglial cells. Transcriptomic analysis revealed expression differences in MHCII complex and phagocytosis-related genes following ethanol exposure; high-PRS microglial cells displayed enhanced phagocytosis and increased *CLEC7A* expression, unlike low-PRS microglial cells. Synapse numbers in cocultures of induced neurons with microglia after alcohol exposure were lower in high-RPS cocultures, suggesting possible excess synapse pruning. This study provides insights into the intricate relationship between AUD PRS, ethanol, and microglial function, potentially influencing neuronal functions in developing AUD.

INTRODUCTION

Alcohol use disorder (AUD) remains a substantial contributor to the global burden of disease, posing an elevated risk for premature mortality and disability (*1*). The etiology of AUD is multifaceted, with genetic factors accounting for approximately half of the inter-individual variation in susceptibility (*2*). This heritable dimension of AUD is highly polygenic (*3*–*6*). Polygenic risk scores (PRS) summarize the combined impact of numerous genetic variants on an individual's risk for specific diseases. AUD PRS captures a fraction of the genetic risk (*7*–*12*), but how that might affect cellular functions is unknown.

Immune and inflammatory pathways in the brain are activated in AUD (*13*). In gene expression profiling of postmortem human brains, a connection between immune responses and AUD has been established; genes exhibiting significant expression differences are enriched in pathways related to interferon signaling (*14*). Interferons—with their antiviral, antiproliferative, and immunomodulatory effects—play a critical role in human innate and adaptive immune responses during chronic alcohol exposure (*14*). Using human induced pluripotent stem cells (iPSCs) as a model system, it has been shown that ethanol exposure activates NLRP3 inflammasome in human iPSCs and iPSC-derived neural progenitor cells (*15*). Microglia are the primary resident immune cells in the brain (*16*) and have a variety of receptors that enable them to sense alterations in their microenvironment, leading to changes in transcription, morphology, and function (*17*, *18*). Brain microglial cells play multifaceted roles, including the regulation of inflammation, participation in phagocytosis (*19*), and engagement in specialized brain-specific functions through interactions with neurons, such as the modulation of neurotransmission and synaptic pruning (*20*, *21*). Exposure to ethanol triggers microglia activation, leading to morphological changes and heightened immune responses in rodent models (*22*–*26*). Microglial depletion has been shown to mitigate alcohol dependence–associated behaviors, impair synaptic function, and reverse expression changes in alcohol-dependent inflammatory-related genes in mice (*27*). It has also been suggested that microglia-mediated synaptic pruning may constitute the underlying mechanism behind synapse loss and memory impairment induced by prolonged alcohol consumption (*28*).

It is increasingly evident that rodent microglia may not faithfully mirror the biology of their human counterparts, as recent transcriptomic studies have revealed substantial differences, including the abundant expression of specific immune genes in human microglia that are not part of the mouse microglial signature (*17*, *29*, *30*). Human microglia can be derived from human iPSCs (*30*–*34*); they serve as an excellent model system for studying neuroimmune interactions (*30*, *35*, *36*). When human iPSCs differentiated into microglia were exposed to brain substrates, including synaptosomes, myelin debris, apoptotic neurons, or synthetic β amyloid fibrils, it resulted in a variety

[1]Department of Neuroscience and Cell Biology and The Child Health Institute of New Jersey, Rutgers Robert Wood Johnson Medical School, New Brunswick, NJ 08901, USA. [2]Department of Biochemistry and Molecular Biology, Rutgers, The State University of New Jersey, 604 Allison Road, Piscataway, NJ 08854, USA. [3]Center for Advanced Biotechnology and Medicine, Rutgers, The State University of New Jersey, 679 Hoes Lane West, Piscataway, NJ 08854, USA. [4]Center for Psychiatric Genetics, NorthShore University HealthSystem, Evanston, IL 60201, USA. [5]Department of Psychiatry and Behavioral Neuroscience, University of Chicago, Chicago, IL 60637, USA. [6]Department of Biochemistry and Molecular Biology, Indiana University School of Medicine, Indianapolis, IN, USA. [7]Department of Psychiatry & Behavioral Sciences, SUNY Downstate Health Sciences University, Brooklyn, NY 11203, USA. [8]Department of Psychiatry, Washinton University School of Medicine, Saint Louis, MO 63108, USA. [9]Nash Family Department of Neuroscience, Icahn School of Medicine at Mount Sinai, New York, NY, USA. [10]Department of Psychiatry, Rutgers University Robert Wood Johnson Medical School, Piscataway, NJ 08854, USA. [11]Human Genetics Institute of New Jersey, Rutgers University, Piscataway, NJ 08854, USA. [12]Department of Genetics, Rutgers University, Piscataway, NJ 08854, USA. [13]Department of Cell Biology & Neuroscience, Rutgers University, Piscataway, NJ 08854, USA.
*Corresponding author. Email: pangzh@rwjms.rutgers.edu

of transcriptional changes (*37*). These changes corresponded to gene signatures found in human brain microglia, particularly those enriched in neurodegenerative diseases (*37*). Therefore, human iPSC-derived microglia could be used as an in vitro model to understand disease-relevant cellular phenotypes. Despite the involvement of microglia in the pathophysiology of AUD (*27*, *38*–*40*), the specific cellular and molecular mechanisms that govern the interaction between ethanol exposure and AUD PRS in the human context remain unknown.

In this study, subject-specific microglia were generated from iPSC lines derived from selected participants with high AUD PRS (high-PRS, $n = 8$, top 75 percentile, five males, three females, all diagnosed with AUD) or low AUD PRS (low-PRS, $n = 10$, bottom 25 percentile, five males and five females, all unaffected). These individuals were from the Collaborative Study on the Genetics of Alcoholism (COGA). COGA has found many genetic and molecular mechanisms underlying the functional alteration in AUD (*41*). We selected subjects with a defined clinical diagnosis of AUD with high-PRS or control samples with low-PRS with no AUD (*12*), which provide a unique opportunity to investigate the gene and environment (i.e., ethanol exposure) interaction and cellular functions. Because PRS summarizes a large number of genomic variations, and there are no consistent variants defining each group, we expected to find a large degree of variability among cell lines within each group. In highly enriched human microglial cells derived from iPSCs, we found that ethanol exposure leads to up-regulation of CD68 expression and alterations in microglial morphology, with distinct effects observed in microglia derived from subjects with different AUD PRS. Transcriptomic analysis unveiled differences between high-PRS and low-PRS microglial cells in the expression of genes related to the major histocompatibility complex (MHC) II complex and to phagocytosis after ethanol exposure. Furthermore, an enhanced phagocytic process with increased *CLEC7A* (C-type lectin domain family 7 member A) RNA expression was observed in high-PRS microglial cells following ethanol exposure, which was not observed in low-PRS microglial cells. Our study reveals the intricate interplay between AUD-related polygenetic factors and microglial function in AUD, offering important insights into the mechanism underlying AUD in humans.

RESULTS

Generation of human iPSC-derived microglia

To test the hypothesis that AUD PRS affects cellular mechanisms, we prepared 18 iPSC lines from lymphocytes and lymphoblastoid cells from participants collected by the COGA (*41*–*43*) based on their AUD PRS (*12*). Eight participants (five men and three women) had AUD and a PRS > 75 percentile (high-PRS, seven of which were above 90 percentile), and 10 (five men, five women) were unaffected participants (no AUD) a PRS < 25 percentile (low-PRS, nine below were 10 percentile) (table S1). The pluripotency of these iPSC lines was validated with immunohistochemical (IHC) staining with pluripotency markers such as Oct4, SOX2, and TRA-160 (fig. S1). Furthermore, we also analyzed chromosomal aberrations by allelic bias using RNA sequencing (RNA-seq) data, i.e., expression-based single nucleotide polymorphism (e-SNP)–karyotyping (*44*) and G-band karyotyping. We found no significant chromosomal aberrations in these iPSC lines ($P < 0.001$; figs. S2 and S3). All COGA iPSC lines can be requested from National Institute on Alcohol Abuse and Alcoholism (NIAAA) (https://cogastudy.org/resources-for-researchers/).

Using an established, highly efficient, and reproducible protocol (*32*), we generated microglial cells from these iPSCs. We first derived primitive macrophage progenitors (PMPs) from iPSCs (Fig. 1, A and B, and table S1). Across multiple iPSC lines, more than 90% of the PMPs exhibited expression of the hematopoietic progenitor cell markers CD235 (Fig. 1, C and D) and CD43 (Fig. 1, E and F). After confirming the PMP cell identities, we differentiated these PMPs into microglial cells by adding interleukin-34 (IL-34) and granulocyte-macrophage colony-stimulating factor (GM-CSF) for 1 week. Microglial identity was confirmed through immunostaining for a panel of microglia-specific markers, including IBA1, P2Y12, CX3CR1, TMEM119, and PU.1 (Fig. 1G).

Differential transcriptomic profiles between high-PRS and low-PRS microglial cells

We conducted bulk RNA-seq analysis in human microglia generated from iPSCs ($n = 9$, four high-PRS, and five low-PRS, both sexes; table S1) (*32*). We first compared the expression levels with a publicly available single-cell RNA-seq dataset of adult human brain cells (*45*). The iPSC-derived microglia and adult human microglial cells show very similar transcriptomic profiles (fig. S4A), indicating the appropriate differentiation of our human microglia.

We identified 1980 differentially expressed genes (DEGs) between high-PRS and low-PRS microglial cells in the absence of ethanol (Fig. 2A). Among these DEGs, the genes with higher expression ($n = 1013$) in AUD high-PRS showed notable enrichment of Gene Ontology (GO) biological process terms related to chromosome separation regulation and mitotic sister chromatid separation (Fig. 2B). In addition, these genes were significantly enriched for receptor activator (Fig. 2C) and cellular component ontologies relating to chromosomes and centromeric regions (Fig. 2D). On the other hand, the genes with lower expression ($n = 967$) in AUD high-PRS exhibited enrichment in biological functions related to immune signaling, specifically involving peptide antigen assembly with the MHCII protein complex and antigen processing and presentation (Fig. 2B). In terms of molecular function, these lower DEGs were predominantly linked to immune receptor activity, antigen binding, and MHCII protein complex binding (Fig. 2C), with their cellular component enrichment observed in the MHCII protein complex (Fig. 2D). Notably, a higher expression level of "chromosome separation" genes in the high-PRS microglial cells was observed when compared with low-PRS microglial cells (Fig. 2E). Also, we noticed lower expression levels of genes belonging to the "antigen processing and presentation" terms in AUD low-PRS cells (Fig. 2F). There was, as expected, considerable variability among individual lines.

Activation of human microglial cells in response to ethanol exposure

To gain insight into the relationship between AUD PRS and ethanol exposure in microglia, we next investigated whether ethanol exposure causes differential cellular responses in human high-PRS ($n = 5$) versus low-PRS ($n = 6$) microglial cells (table S1). We used intermittent ethanol exposure for 7 days, with ethanol replenished daily, as reported previously (*46*). It has been reported that ethanol activates microglial cells in rodents (*47*, *48*). To investigate if ethanol activates human microglia in culture, we assessed the expression of CD68, a transmembrane protein found in plasma, lysosomal, and endosomal membranes that indicates microglial activation (*49*). In both

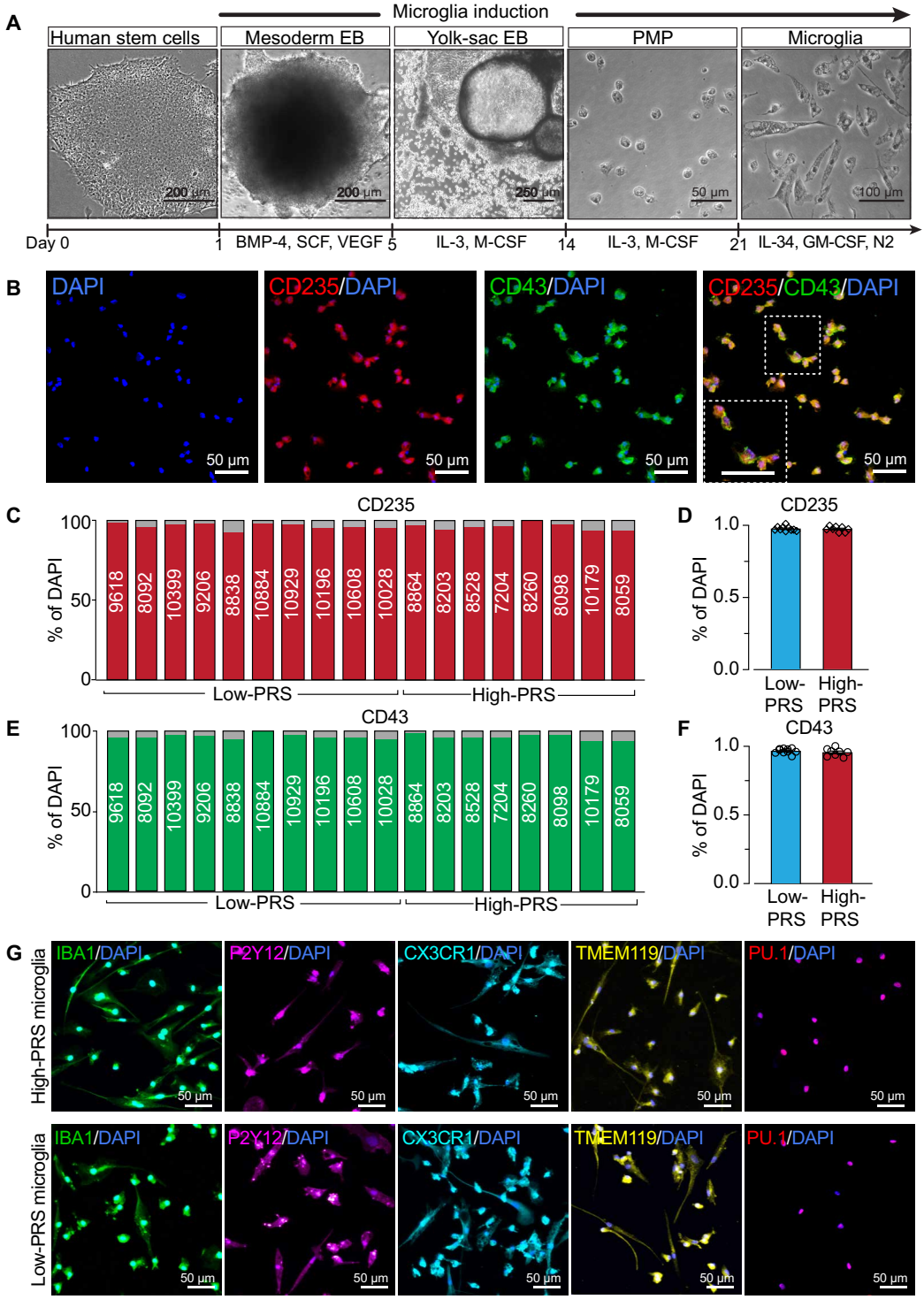

Fig. 1. Characterization of iPSC-derived PMPs and microglia. (**A**) Protocols for generation of PMPs and microglial cells from iPSC. (**B**) Representative images of CD235$^+$ and CD43$^+$ cells in PMPs (line 8864). (**C** and **D**) Quantification of CD235$^+$ PMPs derived from all iPSC lines with different PRS (low-PRS, $n = 10$; high-PRS, $n = 8$). (**E** and **F**) Quantification of CD43$^+$ PMPs derived from all iPSC lines with different PRS (low-PRS, $n = 10$; high-PRS, $n = 8$). (**G**) Representative images of IBA1$^+$, P2Y12$^+$, CX3CR1$^+$, TMEM119$^+$, and PU.1$^+$ microglia from high-PRS line 8864 and low-PRS line 9618. BMP-4, bone morphogenetic protein 4; VEGF, vascular endothelial growth factor; EB, embryonic body; SCF, stem cell factor; IL-3, interleukin-3; M-CSF, macrophage colony stimulating factor; IL-34, interleukin-34; GM-CSF, granulocyte-macrophage colony stimulating factor; DAPI, 4′,6-diamidino-2-phenylindole.

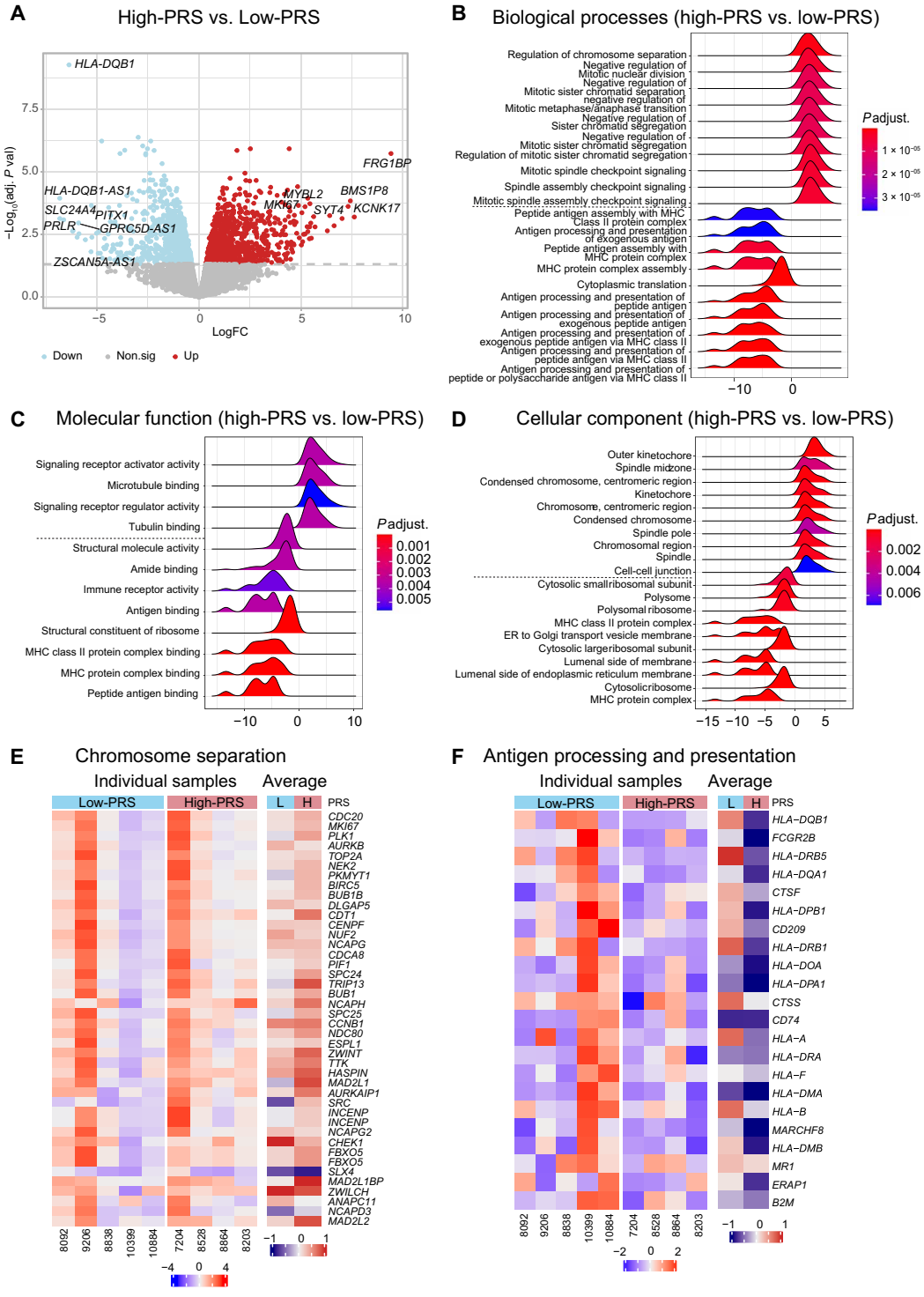

Fig. 2. Whole-genome transcriptome profile comparison between human microglial cells derived from high-PRS and low-PRS iPSC lines. (**A**) Volcano plot depicts the DEGs between the high-PRS and low-PRS microglial cells. (**B** to **D**) GO analysis depicting the significant terms (top 10 up- and down-regulated terms) associated with microglia when comparing high-PRS versus low-PRS. It includes biological processes (BPs, B), molecular functions (MFs, C), and cellular components (D). *P* adjusted values are displayed. (**E**) Heatmap illustrates gene expression patterns related to chromosome separation in both high-PRS (red, $n = 4$ lines) and low-PRS (blue, $n = 5$ lines) microglia. (**F**) Heatmap illustrates gene expression patterns related to antigen processing and presentation in both high-PRS (red, $n = 4$ lines) and low-PRS (blue, $n = 5$ lines) microglia.

high-PRS and low-PRS human microglial cells, we observed elevated expression of CD68 after ethanol exposure (Fig. 3, A and B). The level of ethanol-induced CD68 expression was similar between high-PRS and low-PRS microglial cells (Fig. 3, A and B). Because activated microglia undergo morphological changes from a "ramified" state, a highly branched and elongated appearance, to an "amoeboid" state, with retracted processes and a more rounded shape (*50*), we used "fractal analysis" in ImageJ at the single-cell level to evaluate human microglial morphology (Fig. 3C and fig. S4B). In the absence of ethanol, high-PRS microglial cells displayed lower fractal dimension values and higher circularity compared to low-PRS microglial cells (Fig. 3D and fig. S4, C to E). Following ethanol exposure, there was a reduction in fractal dimension observed in both high-PRS and low-PRS microglial cells (Fig. 3D), indicating a decrease in the complexity of microglial morphology in response to ethanol exposure. Notably, high-PRS microglial cells exhibited a more significant decrease in fractal dimension and spine ratio, alongside a marked increase in circularity relative to their low-PRS counterparts after exposure to ethanol. These observed differences were notably more substantial under the 75 mM ethanol condition (Fig. 3D). These data indicated that human microglial cells were activated by ethanol exposure, and there are differences in morphological features between high-PRS and low-PRS microglial cells, suggesting that genetic background may affect cellular responses to ethanol.

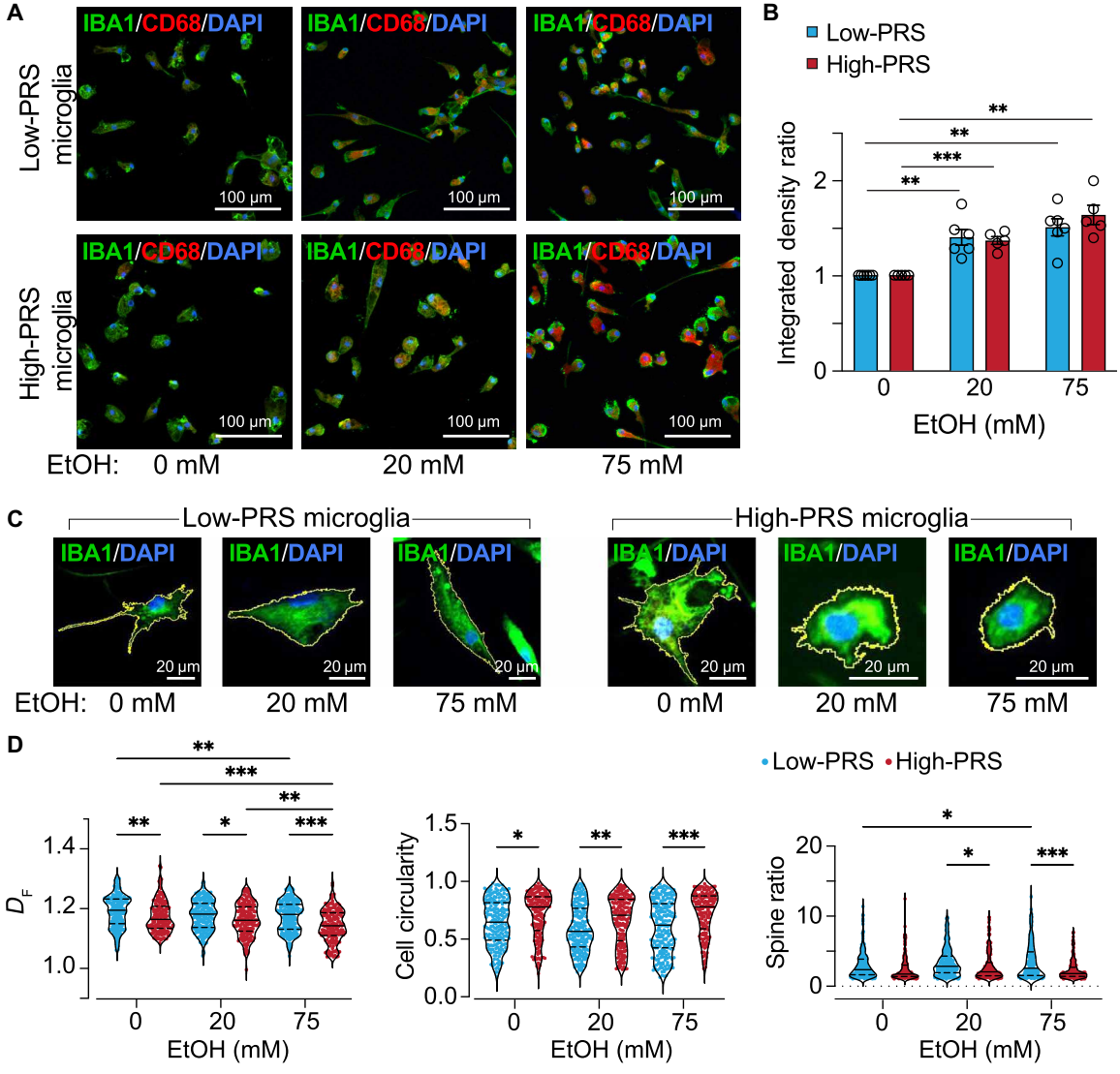

Fig. 3. The impact of ethanol exposure on the activation of iPSC-derived microglia. (**A**) Representative images of $CD68^+$ and $IBA1^+$ microglia derived from high-PRS (line 8528) and low-PRS lines (line 9206) following a 7-day exposure to ethanol (0, 20, and 75 mM). (**B**) Quantification of CD68 corrected fluorescence-integrated density normalized to each control (0 mM) replicate. Low-PRS ($n = 6$ lines) versus high-PRS ($n = 5$ lines), $^{**}P < 0.01$ and $^{***}P < 0.001$. Data are presented as mean ± SEM. (**C**) Representative images showing the process traced with regions of interest (ROI) using the IBA1 signal in iPSC-derived microglia with high-PRS (line 8864) or low-PRS (line 8838). (**D**) Morphological analysis of microglia binary outlines using FracLac ImageJ. $n = 177$ cells in five high-PRS lines, 211 cells in six low-PRS lines for 0 mM; $n = 188$ cells in five high-PRS lines, 214 cells in six low-PRS lines for 20 mM; $n = 164$ cells/five high-PRS lines, 219 cells/six low-PRS lines for 75 mM. $^*P < 0.05$, $^{**}P < 0.01$, and $^{***}P < 0.001$. Data are presented as medium ± quartiles.

Transcriptomic profile differences of high-PRS and low-PRS microglial cells in response to ethanol exposure

We next determined the effects of intermittent ethanol exposure on the transcriptomic profiles of the iPSC-derived microglia ($n = 9$, four high-PRS and five low-PRS; table S1). Exposure to ethanol did not affect human microglial cell identity, as determined by comparing our microglial bulk RNA-seq data with the publicly available single-cell RNA-seq dataset of adult human brain cells (fig. S4A) (*45*). Some *ADH* and *ALDH* genes—including *ADH5*, *ALDH1A1*, *ALDH1A2*, and *ALDH2*—which encode enzymes involved in metabolizing ethanol into acetaldehyde and acetate (*51*), were found to be expressed by human microglia (table S2), suggesting that they may metabolize ethanol.

To investigate the different impacts of intermittent ethanol exposure on the transcriptomic profiles, we compared gene expression profiles with and without ethanol exposure (0 mM versus 75 mM) (table S1). We identified 3169 DEGs associated with intermittent ethanol exposure in high-PRS microglial cells and 2472 DEGs in low-PRS microglial cells (Fig. 4, A and B). Among these DEGs, 1601 were up-regulated in high-PRS microglial cells, while 1308 were up-regulated in low-PRS microglial cells after intermittent ethanol exposure, with 909 genes overlapping between high-PRS and low-PRS microglial cells (fig. S5). GO analysis unveiled significant enrichment of terms from the up-regulated DEGs in high-PRS lines, but not in low-PRS lines, in biological processes related to peptide antigen assembly with the MHCII protein complex and antigen processing and presentation (Fig. 4, C and D). Subsequently, we plotted running scores from gene set enrichment analysis (GSEA) explicitly focusing on the GO biological process terms unique to high-PRS microglial cells. In addition to the terms related to antigen processing and presentation via the MHCII protein complex, this analysis uncovered significant enrichment of terms related to the regulation of phagocytosis (Fig. 4, E and F). This observation underscores the impact of ethanol on antigen presentation, a critical process closely tied to phagocytosis, which encompasses the uptake, processing, and presentation of antigens to initiate adaptive immune responses.

Genes related to antigen processing and presentation are shown in Fig. 5A, and genes associated with phagocytosis in Fig. 5C. Most of these genes showed a significant increase in expression in high-PRS microglial cells following exposure to ethanol. In contrast, their expression levels remained relatively stable in low-PRS microglial cells (Fig. 5, B and D). Notably, one of the genes identified in this category, *CLEC7A* [Dectin-1, encoding a mammalian C-type lectin receptor expressed on microglial cell surfaces that is known to promote zymosan phagocytosis (*52*)], exhibited substantial up-regulation in high-PRS microglial cells after ethanol exposure (Fig. 5D). To validate these findings, we performed immunohistochemistry to assess the expression of CLEC7A protein by immunostaining in each of the 18 cell lines individually (Fig. 6A and table S1). In agreement with mRNA measurements, we found a notable increase in CLEC7A immunoreactivity expression levels in high-PRS microglial cells following ethanol exposure (75 mM). In contrast, the levels remained relatively stable in low-PRS microglial cells (Fig. 6, B and C).

Down-regulated genes affected by intermittent ethanol exposure in high-PRS and low-PRS microglial cells have similar predicted functions. They are significantly enriched in cell cycle regulation, including chromosome separation and mitotic sister chromatid separation (Fig. 4, C and D). To better visualize the gene expression changes in ethanol-responsive DEGs and cell cycle phases in both low-PRS and high-PRS microglial cells, we generated a heatmap summarizing the expression of cell cycle–related genes (fig. S6A). Upon ethanol exposure, the pathway analyses for the up-regulated genes showed enrichment in the G_1-S and G_2-M DNA damage checkpoint markers (figs. S6B and S7). This suggests that ethanol may cause cell cycle arrest and/or DNA damage in high-PRS and low-PRS microglial cells. An increase in γ-H2AX [a sensitive molecular marker of DNA damage (*53*)] after exposure to 75 mM ethanol was found by immunostaining in both high-PRS and low-PRS microglial cells (fig. S6, C and D). Consistent with a previous report in mouse neurons (*54*), these results indicated that intermittent ethanol exposure may cause DNA damage in human microglia, potentially interfering with microglial proliferation.

Differential phagocytic function in high-PRS and low-PRS human microglial cells after intermittent ethanol exposure

As noted above, high-PRS and low-PRS microglial cells showed differential morphological changes and differential gene expression, particularly up-regulation of genes related to phagocytosis, in high-PRS microglial cells following intermittent ethanol exposure. Thus, we hypothesized that high-PRS and low-PRS would show differential phagocytosis after intermittent ethanol exposure. To test this hypothesis, we used pH-sensitive pHrodo zymosan beads to assess the phagocytic activity (*55, 56*) in microglial cells derived from 18 lines individually, both with high-PRS and low-PRS, after 7-day intermittent ethanol exposure at two different ethanol concentrations (20 and 75 mM; Fig. 7, A and B). At baseline (ethanol-free), we did not observe a significant difference between high-PRS and low-PRS in the integrated density of zymosan beads within the microglial cells (Fig. 7C). However, we did notice a higher proportion of microglia containing beads in low-PRS microglial cells compared to high-PRS microglial cells without ethanol exposure (Fig. 7D). Following intermittent ethanol exposure, we observed significantly augmented phagocytosis in high-PRS microglial cells, particularly at higher ethanol concentrations (75 mM) (Fig. 7, B and C), while low-PRS cells did not exhibit a corresponding increase (Fig. 7, A and C). A similar pattern was observed in the proportion of microglia containing beads, which substantially increased in high-PRS microglial cells but remained relatively unchanged in low-PRS microglial cells after intermittent ethanol exposure (Fig. 7D). Our results indicated that ethanol exposure enhances phagocytic activity in high-PRS, but not in low-PRS microglial cells. These results suggested a potential link between variation in genetic background summarized by PRS and ethanol-induced alterations in microglial function.

Because it has been suggested that microglia interact with neurons through synaptic pruning to shape synapse formation and synaptic transmission (*20*, *21*), we also assayed microglial phagocytosis using isolated synaptosomes of human induced neurons [iNs; induced by ectopic expression of the transcription factor neurogenin 2 (Ngn2)] (*57*), which contains synaptic proteins such as PSD 95 and SNAP receptor proteins (fig. S8, A and B). These synaptosomes were labeled with pH-sensitive pHrodo dye and were added to both high-PRS and low-PRS microglial cultures after a 7-day intermittent ethanol exposure at 75 mM (fig. S8C). Consistent with the results from the beads phagocytosis assay, we also observed that high-PRS microglial cells exhibited enhanced phagocytic activity toward synaptic proteins after ethanol exposure, demonstrated by higher fluorescence intensity and the proportion of microglia containing synaptic proteins (fig. S8, D and E). Notably, this enhanced phagocytic activity was reversible upon treatment with phagocytosis inhibitors such as minocycline and cytochalasin D (fig. S8, C to E).

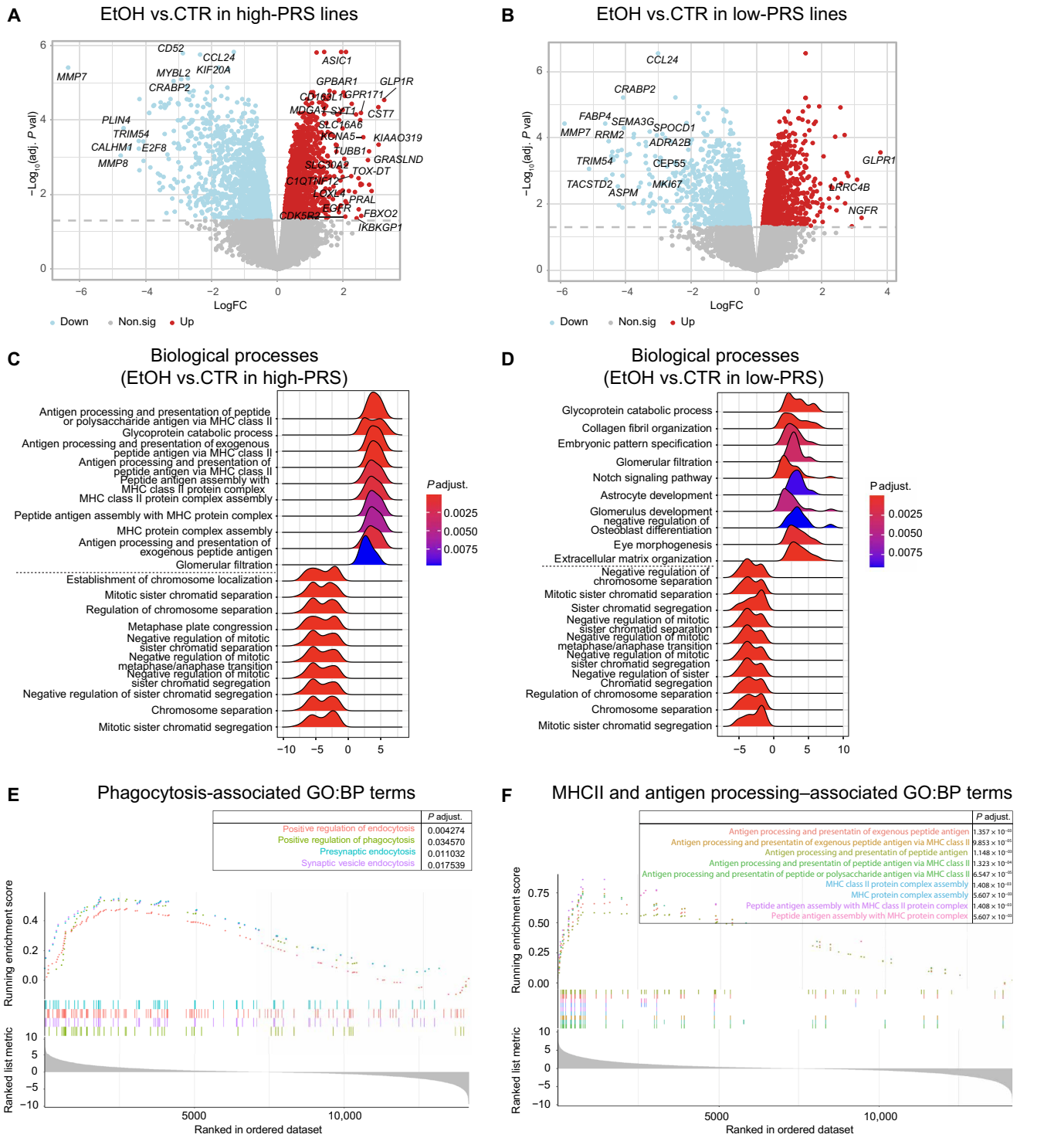

Fig. 4. Transcriptomic profiles in high-PRS versus low-PRS human microglia after ethanol exposure. (**A** and **B**) Volcano plots depict the DEGs between the different ethanol concentrations (75 mM versus 0 mM) in four high-PRS lines (A) and five low-PRS lines (B) of microglial cells. (**C** and **D**) GO analysis of BPs highlighting significant terms (top 10 up- and down-regulated terms) associated with ethanol exposure (75 mM versus 0 mM) in both high-PRS (C) and low-PRS (D) microglia. Adjusted *P* values (*P* adjust.) are displayed. (**E**) GSEA plot depicting the enrichment of the phagocytosis-associated pathway specific to high-PRS microglia following ethanol exposure. *P* values and *P* adjust. are displayed. (**F**) GSEA plot of the MHCII and antigen processing–associated pathway enrichment specific to high-PRS microglia following ethanol exposure. *P* values and *P* adjust. are displayed.

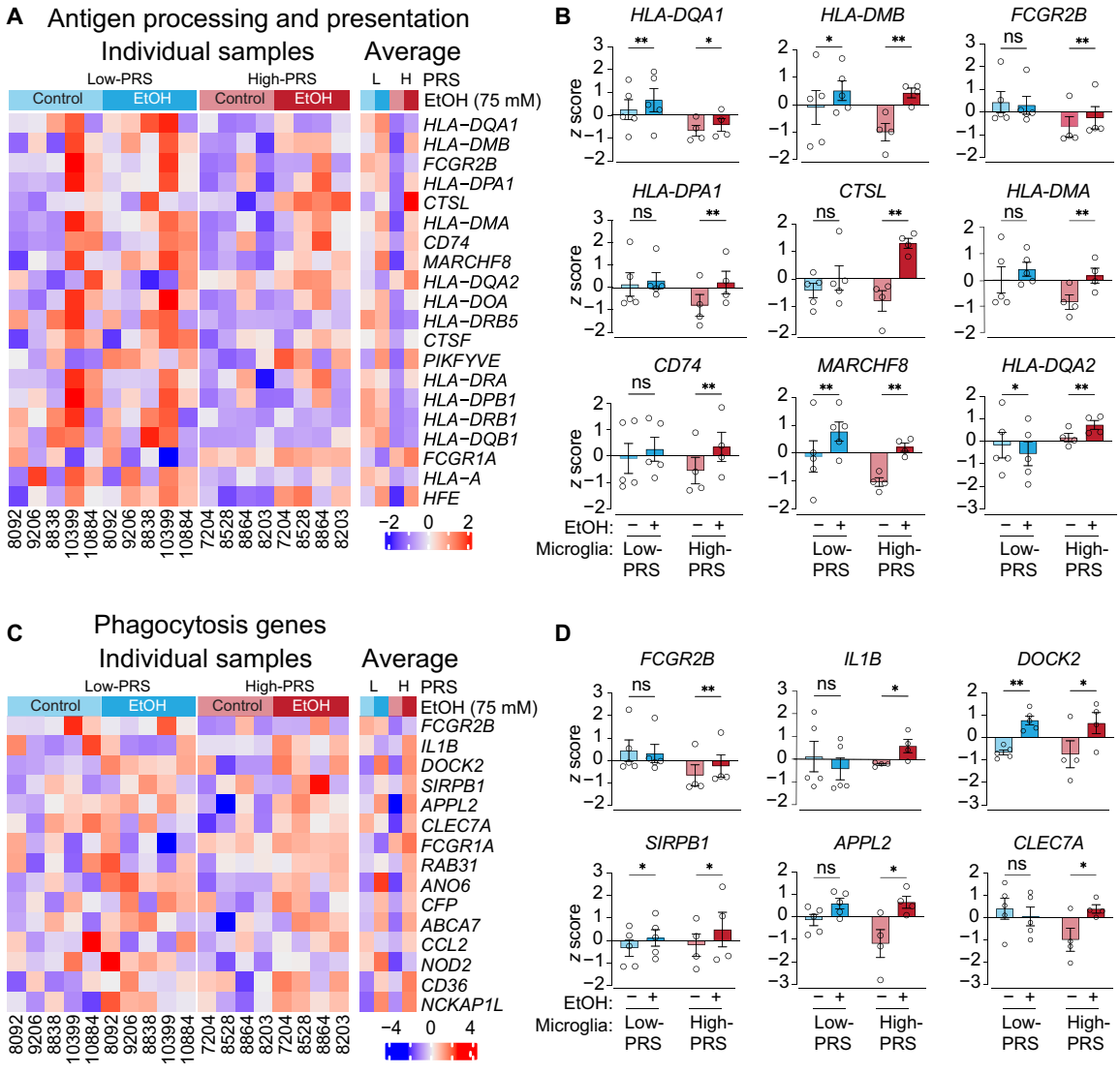

Fig. 5. Differential expression of phagocytosis-related genes between high-PRS and low-PRS microglia in response to ethanol exposure. (**A**) A heatmap illustration of the gene expression profiles related to antigen processing and presentation in both high-PRS (red) and low-PRS (blue) microglia, with and without ethanol exposure. (**B**) Box blots comparisons of the differential expression of genes associated with antigen processing and presentation in microglia from both high-PRS (red) and low-PRS (blue) lines, with and without ethanol exposure. Low-PRS/high-PRS lines = 5/4. *$P < 0.05$ and **$P < 0.01$. Data are presented as means ± SEM. (**C**) A heatmap illustration of the gene expression profiles related to the phagocytosis pathway in both high-PRS (red) and low-PRS (blue) microglia, with and without ethanol exposure. (**D**) Box blots comparison of the representative differential expression of genes associated with the phagocytosis pathway in microglia from both high-PRS (red) and low-PRS (blue) lines, with and without ethanol exposure. Low-PRS/high-PRS lines = 5/4. *$P < 0.05$ and **$P < 0.01$. Data are presented as means ± SEM.

We thus examined the impact of microglial cells with high and low AUD-PRS on human iPSC-derived neurons. We individually cocultured each line of microglial cells (six lines of high AUD PRS and seven lines of low AUD PRS; see table S1 for detail) with induced human iNs. The iNs were induced from an iPSC line with no diagnosed AUD, as used in a previous study (*58*). Thereby, we were able to evaluate the differential effects between high-PRS and low-PRS microglia on a common set of "neutral" neurons. To facilitate synapse formation, these iNs were cultured on monolayer mouse glial cells (*59, 60*). High-PRS or low-PRS microglial cells were added to iN cultures on day 14 after induction. The final microglial density in culture (days 35 to 40 after induction) is around 7 to 9% of total cell numbers, including mouse glial cells (Fig. 8, A and B), which is consistent with the microglia proportion in the human brain (*61*). We first analyzed synapse formation after a 7-day intermittent ethanol exposure with 75 mM ethanol. After IHC staining with the presynaptic marker synapsin and the neuronal marker MAP2, we used Intellicount (*62*) to quantify the synaptic density per cell. As a control, we also included iN cultures (on mouse glia) without microglia. We found that synaptic density was increased in human iN cultures after intermittent ethanol exposure (Fig. 8, C and D). While adding low-PRS microglial cells had no substantial impact on the synaptic density, high-PRS microglial cells reversed the increase of synapse number after intermittent ethanol exposure (Fig. 8, C and D). To further validate the impact of high-PRS microglial cells on synaptic formation/function, we conducted patch-clamp electrophysiology on iNs with or without microglial cells. Consistent with the findings of the

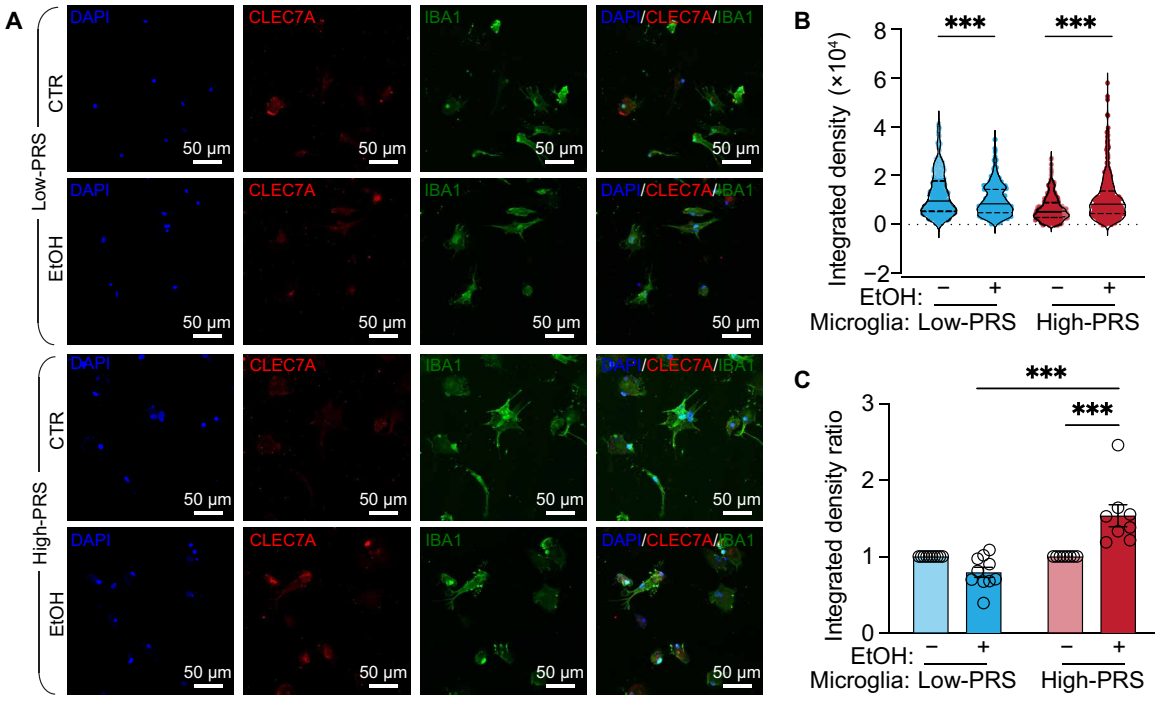

Fig. 6. CLEC7A expression between high-PRS and low-PRS microglia after ethanol exposure. (**A**) Representative images of CLEC7A$^+$ and IBA1$^+$ microglia derived from PRS lines following ethanol exposure (0 and 75 mM). (**B** and **C**) Quantification of CLEC7A$^+$ fluorescence-integrated density (B) and corrected fluorescence-integrated density normalized to each control (0 mM) replicate (C). $n = 331$ cells/eight high-PRS lines and 365 cells/10 low-PRS lines for 0 mM; $n = 315$ cells/eight high-PRS lines and 373 cells/10 low-PRS lines for 75 mM; ***$P < 0.001$. Data are presented as means ± SEM.

synaptic density analyses, after intermittent ethanol exposure, we found increased frequencies of miniature excitatory postsynaptic currents in iNs without human microglia or with low-PRS microglial cells but not in high–PRS-iN cocultures (Fig. 8, E and F).

Together, these findings suggest that ethanol partially induced adaptive changes in the strength of excitatory transmission by increasing synapse numbers in human neurons. AUD high-PRS microglial cells may attenuate the impact of these phenotypic changes through heightened synaptic pruning/elimination activity after ethanol exposure.

DISCUSSION

AUD is a complex genetic disorder, and although most individual genetic variants do not have genome-wide notable effects when considered collectively in a PRS, they quantify part of an individual's susceptibility to developing the disorder (*63*–*65*). We investigated how the polygenic background, represented as PRS, affects microglial function; how intermittent exposure to ethanol affects microglial function; and how the two factors interact. It is likely that many of the genetic variants summarized in PRS can be predicted to affect gene regulatory networks either directly or indirectly. In the absence of ethanol, we found significant DEGs when comparing microglia from individuals with AUD and a high PRS for AUD (i.e., high-PRS) to those from individuals without AUD and with low PRS (i.e, low-PRS). The genes more highly expressed in high-PRS microglial cells were enriched in pathways related to receptor activation and chromosome separation, while those expressed at lower levels were enriched in genes related to immune signaling, particularly with the MHCII complex.

Following intermittent ethanol exposure, we found that high-PRS and low-PRS microglial cells rapidly transition from their default branched profile (*66*) to a more amoeboid state (*67*). Microglia with high-PRS showed a significant decrease in fractal dimension and a pronounced increase in circularity compared to their low-PRS counterparts after ethanol exposure. Further gene expression profiling revealed ethanol exposure alters notable DEGs in high-PRS and low-PRS microglial cells, with more than half of the DEGs overlapping. The up-regulated genes in high-PRS were enriched for processes related to peptide antigen assembly with the MHCII protein complex and antigen processing and presentation, as well as phagocytosis. Microglia, functioning as antigen-presenting cells, are equipped with phagocytic receptors that facilitate the capture of antigens. These antigens undergo processing within phagosomes and are subsequently presented by MHCII and costimulatory molecules expressed in microglia (*68, 69*). The whole process could modulate the immune responses within the central nervous system during AUD.

Among those up-regulated genes, we found significant changes in *CLEC7A* in high-PRS microglial cells at both the transcript and protein levels following exposure to ethanol. CLEC7A is a receptor located on the surface of microglial cells, which plays a crucial role in the immune response by detecting Zymosan, a type of fungal β glucan, and subsequently initiating the phagocytic process in microglia (*52, 70, 71*). This heightened CLEC7A expression in high-PRS microglial cells may partially explain the increased phagocytic activity following exposure to ethanol. In addition, studies have identified *CLEC7A* as a prominent member of the disease-associated microglia genes (*72*), consistently showing elevated expression by microglia in diverse mouse models of neurodegeneration, including Alzheimer's disease

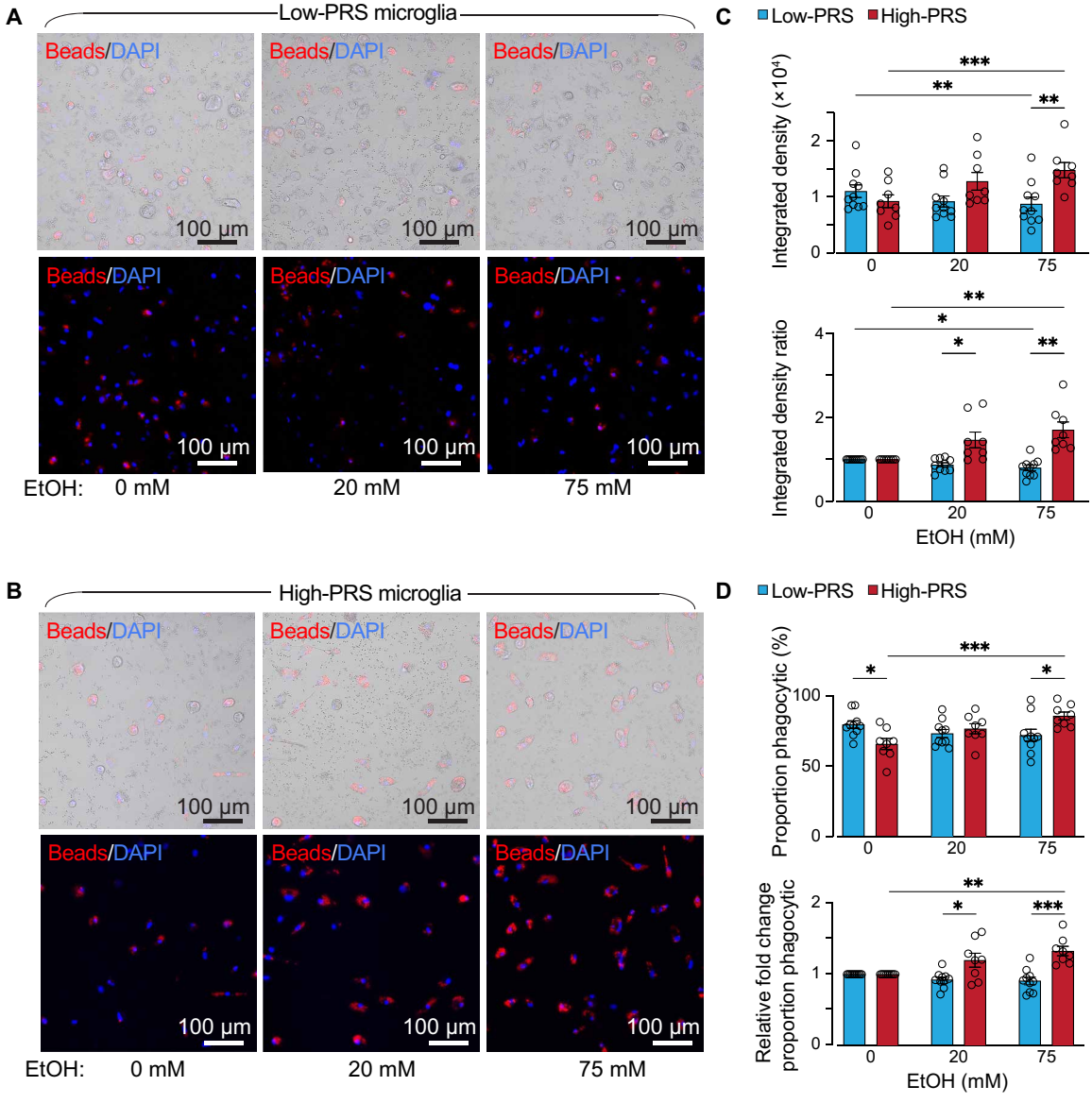

Fig. 7. Enhanced phagocytosis ability in high-PRS iPSC-derived microglia in response to ethanol. (**A** and **B**) Representative live-cell imaging of iPSC-derived microglia from low-PRS (line 8092, A) and high-PRS (line 8528, B) engaged in the phagocytosis of zymosan particles at different ethanol concentrations (0, 20, and 75 mM). The upper images are overlapped with bright-field microscopy for reference. (**C**) Quantification of the fluorescence-integrated density of zymosan bioparticles (beads): The top panel shows the fluorescence-integrated density between high-PRS and low-PRS microglial cells, while the bottom panel shows the corrected fluorescence-integrated density normalized to each control (0 mM). Low-PRS/high-PRS lines = 10/8, $^{**}P < 0.01$ and $^{***}P < 0.001$. Data are presented as means ± SEM. (**D**) Quantification of the proportion of microglia with zymosan particles (beads): The top panel shows the proportion of microglia with beads, while the bottom panel displays the corrected proportion, which has been normalized to each control (0 mM) replicate. Low-PRS/high-PRS lines = 10/8, $^{**}P < 0.01$ and $^{***}P < 0.001$. Data are presented as means ± SEM.

(AD) models (*73*, *74*). Thus, our observation may also suggest a potential connection between the elevated CLEC7A in high-PRS microglial cells and AUD-related dementia. In a recent study, they observed notable differences in the expression of genes associated with human AD among AD mice with various genetic backgrounds. Specifically, the B6.APP/PS1 and WSB.APP/PS1 strains displayed higher expression levels for the gene *CLEC7A*, while the CAST and PWK strains did not (*75*). These results suggest that genetic background may modulate microglial phagocytic function in response to ethanol and influence neuron function in AUD, potentially affecting the interaction between microglia and neuronal cells in the context of AUD pathophysiology.

Microglia can modulate synapses through processes such as partial phagocytosis of synaptic segments or engulfing entire pre- or postsynaptic elements (*76*, *77*). After observing that ethanol can promote microglial phagocytosis of zymosan and synaptoneurosomes in high-PRS lines, we began to investigate the potential effects of high-PRS microglial cells on synaptic transmission in the context of alcohol consumption. To explore this further, we established a coculture system incorporating human Ngn2-iNs and microglia. Our findings

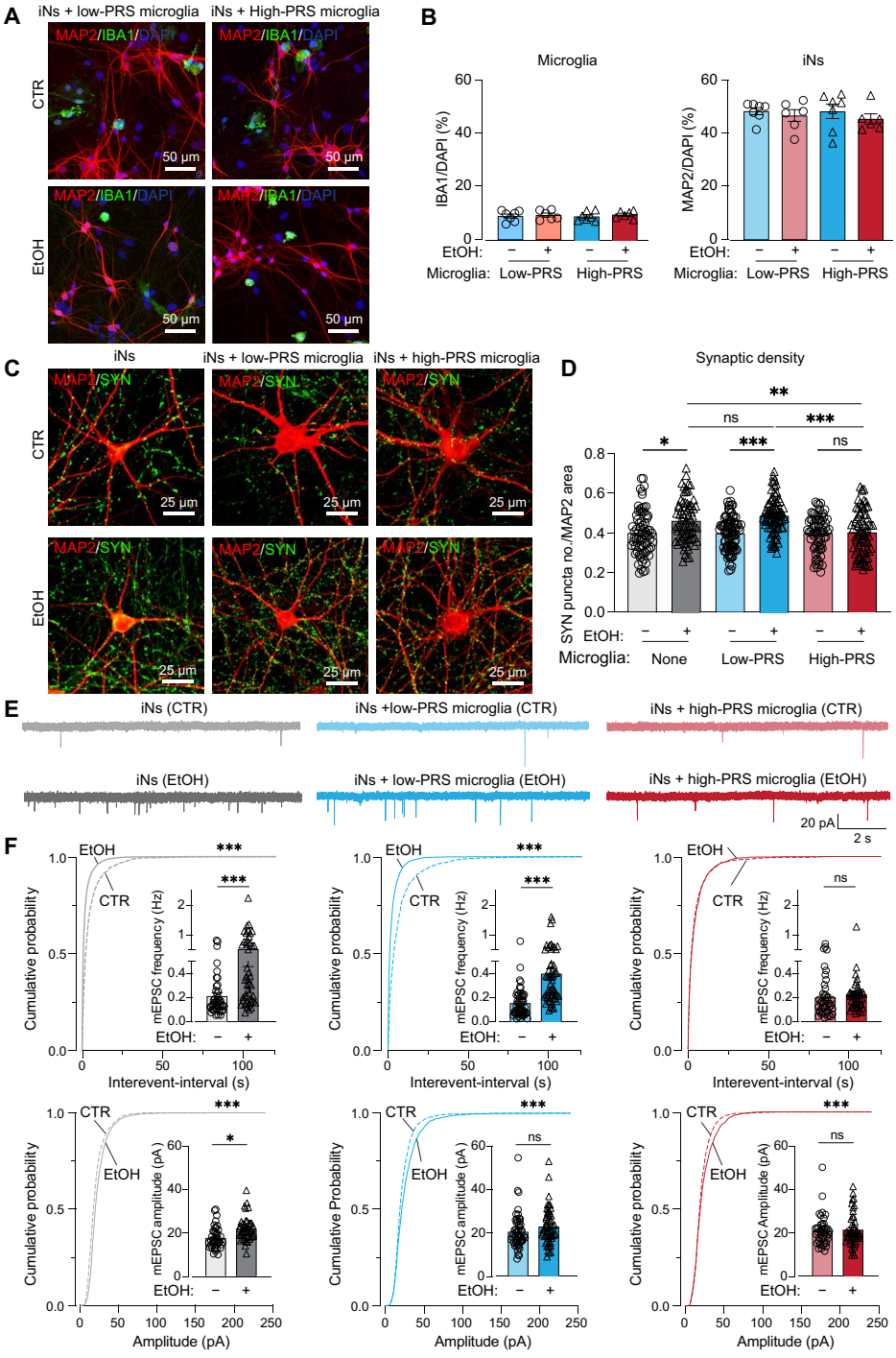

Fig. 8. High-PRS iPSC-derived microglia decreases excitatory neurotransmission in coculture. (**A**) Representative images of coculture consisting of MAP2$^+$ neurons and IBA1$^+$ microglia derived from both high-PRS and low-PRS lines, following treatment with ethanol (0 and 75 mM). (**B**) Quantification of the proportion of microglia and neurons in coculture with high-PRS and low-PRS microglial cells under 0 and 75 mM conditions (low-PRS = 7 lines, high-PRS = 6 lines). Data are presented as means ± SEM. (**C**) Representative images illustrating synaptic puncta (green, labeled by synapsin immunofluorescence) associated with dendrites (red, visualized by MAP2 immunofluorescence) in iNs without microglia, with low-PRS microglial cells or with high-PRS microglial cells. (**D**) Quantification of synapsin puncta densities per MAP2 area. (iN without microglia: 0 mM = 73 images, 75 mM = 73 images; iN + low-PRS microglial cells: 0 mM = 93 images, 75 mM = 85 images; iN + high-PRS microglial cells: 0 mM = 70 images, 75 mM = 75 images). (**E**) Representative traces of miniature excitatory postsynaptic currents (mEPSCs) in Ngn2-iNs without microglia (gray, 0 mM = 43 cells, 75 mM = 46 cells), Ngn2-iNs with low-PRS microglial cells (blue, 0 mM = 53 cells, 75 mM = 55 cells), and Ngn2-iNs with high-PRS microglial cells (red, 0 mM = 43 cells, 75 mM = 46 cells). (**F**) Cumulative distribution and quantification (inserts) of mEPSC frequency (top) and amplitude (bottom) in Ngn2-iNs without microglia (gray), Ngn2-iNs with low-PRS microglial cells (blue), and Ngn2-iNs with high-PRS microglial cells (red). Data are means ± SEM; statistical significance (*$P < 0.05$, **$P < 0.01$, and ***$P < 0.001$) was evaluated with the Kolmogorov-Smirnov test (cumulative probability plots) and *t* test (bar graphs).

indicated that ethanol enhances excitatory synaptic transmission, which aligns with previous research demonstrating increased glutamatergic activity following chronic alcohol exposure (*78*). While we did not observe significant changes in synaptic densities in neurons cocultured with microglia compared to neurons without microglia, we did notice that high-PRS microglial cells may contribute to a reduction in excitatory synaptic densities and transmission in neurons following intermittent ethanol exposure. This suggests that high-PRS microglial cells may play a crucial role in shaping synaptic connectivity through a process known as microglia-dependent synapse elimination, specifically in high-PRS individuals, potentially rendering them at higher risk for developing/maintaining AUD. A mouse study (*28*) has shown that long-term alcohol exposure activates microglia to phagocytose synapses, leading to impaired synaptic plasticity and cognitive function (*47*). Nevertheless, the interactions with heterogeneous neuronal populations in various brain regions further emphasize their diverse contributions to neuronal homeostasis and behavioral regulation, which may be involved in AUD pathophysiology (*79*). Consequently, our results imply that the heightened phagocytic activity observed in high-PRS microglial cells after ethanol exposure may exert a considerable influence on synaptic connectivity and remodeling, potentially affecting neuronal function in the context of AUD-related dementia.

More studies are required to explore how ethanol exposure regulates gene expression in human microglial cultures and how AUD PRS influences the gene expression and functionality of microglial cells. Alcohol can also directly activate microglial cells to increase the production of proinflammatory chemokines and cytokines, which may regulate gene expression in microglial cells (*80*). Neurons can metabolize ethanol into acetate (*54*), but whether microglial cells can produce acetate and highly reactive acetaldehyde from ethanol remains to be investigated. Nevertheless, human microglial cells produced from iPSCs express multiple *ADH* and *ALDH* genes necessary to participate in the metabolic process for ethanol (table S2). The ethanol metabolite acetate can be a crucial source of acetyl-CoA produced by chromatin-bound acetyl-CoA synthetase, essential for histone acetylation and epigenetic regulation for gene expression (*81*). It is also possible that the excessive alcohol consumption in the AUD high-PRS subjects that the high-PRS iPSCs were derived from carried certain epigenetic changes that confer the differences between gene expression and functional differences between the high-PRS versus low-PRS microglial cells. How AUD and PRS may interact with histone acetylation, as affected by ethanol metabolites and open chromatin state to influence gene expression in vivo and in vitro, needs to be further elucidated.

It is important to acknowledge certain limitations in our study. Notably, our experimental approach relied on a two-dimensional cell culture, which, while valuable for investigating microglial responses and gene expression patterns, does not recapitulate the complex three-dimensional interactions that occur in the brain and in vivo. The specific mechanisms by which microglia detect and respond to ethanol are still not fully understood. Moreover, it should be recognized that cultured cells incubated with ethanol do not fully replicate microglia in humans with chronic alcohol consumption. Further investigations using brain organoid models (*32*) or in vivo (*30*) studies will help gain a more comprehensive understanding of the dynamics and functional consequences of microglia-neuron interactions in AUD and the role of genetic factors in these interactions. Our current study did not specifically investigate the mechanisms of interaction between genetic risk factors and environmental influences, which are crucial in determining an individual's susceptibility to AUD. Polygenic and environmental risks often reinforce each other (*82*). Factors such as family dynamics, peer interactions, adverse life events, and broader societal factors such as religion and education interact with genetic predispositions to pronouncedly affect individual drinking behaviors and susceptibility to AUD (*83*). Future studies of polygenic risk mechanisms should attempt to incorporate environmental factors to provide a more comprehensive understanding of AUD susceptibility.

In this study, we conducted a 7-day exposure to ethanol, and thus, we could not assess the effects of long-term heavy drinking in the high PRS or low PRS group. In addition, the subjects' cells were reprogrammed. The experimental system we used exposed newly generated and naive microglia with different genetic backgrounds to "toxic" concentrations of ethanol (but not long term). Although the high AUD PRS subjects were diagnosed with AUD, and the low PRS subjects were not, our study likely could not provide insight into whether a prior history of alcohol drinking interacts with PRS to affect the microglial phenotype in vitro after ethanol exposure. Therefore, we focused on the a priori genetic risk factors and observed changes in gene expression in high PRS microglia, indicating a neuroimmune response. These same changes in microglia may occur in individuals at risk with long-term heavy drinking, but further studies are needed to assess this possibility.

In summary, we observed differential gene expression patterns in high-PRS and low-PRS human microglial cells in response to intermittent ethanol exposure and heightened phagocytotic responses in the AUD high-PRS microglial cells that may affect synaptic transmission differentially than low-PRS microglial cells. These findings shed light on the multifaceted mechanisms underlying AUD and emphasize the importance of considering genetic factors when exploring microglial responses in this complex disorder.

MATERIALS AND METHODS

Human iPSC lines

The human iPSC lines used in this study were derived from lymphocytes and lymphoblastoid cells collected from the COGA study participants obtained from the NIAAA/COGA Sharing Repository. These samples are deidentified. The selection criteria for these individuals were based on previously established PRS for AUD (*12*). Specifically, to investigate PRS for AUD, we selected eight individuals diagnosed with AUD according to the Diagnostic and Statistical Manual, fifth edition (*84*) with PRS greater than the 75th percentile and 10 individuals who had no history of AUD and exhibited PRS lower than the 25th percentile (table S1). Cryopreserved lymphocytes were thawed, and the erythroblastic cells expanded and infected with the Sendai virus, expressing reprogramming factors (CytoTune, Life Technologies). All reprogramming and assessment of pluripotency was performed by Sampled, formerly Infinity BiologiX LLC. Cultures of iPSC were maintained feeder free on Matrigel Matrix (Corning Life Sciences, catalog no. 354234) in mTeSR plus medium (STEMCELL Technologies, catalog #100-0276) and routinely passaged with Accutase (STEMCELL Technologies, catalog #07920). The experiments were done under the Rutgers Biosafety protocol #13-444.

Differentiation and culture of human iPSC-derived PMPs and microglia

PMPs were derived from iPSC lines using an established protocol (*32*). To initiate the formation of yolk sac embryoid bodies (YS-EBs),

we exposed them to mTeSR plus medium supplemented with bone morphogenetic protein 4 (BMP4) (50 ng/ml; PeproTech, catalog #120-05ET), vascular endothelial growth factor (VEGF) (50 ng/ml; PeproTech, catalog #100-20A), and stem cell factor (SCF) (20 ng/ml; PeproTech, catalog #300-07) for 6 days. For the induction of myeloid differentiation, YS-EBs were plated onto 10-cm dishes containing X-VIVO 15 medium (Lonza, catalog #02-060Q) supplemented with interleukin-3 (IL-3) (25 ng/ml; PeproTech, catalog #200-03) and macrophage colony stimulating factor (M-CSF) (100 ng/ml; PeproTech, catalog #200-25) (*34, 85*). Human PMPs emerged in the supernatant after 4 weeks after plating and maintained production for over 6 months.

To achieve full maturation of microglia, we subjected the PMPs to a carefully designed 7-day treatment regimen. This involved the addition of interleukin-34 (IL-34) (100 ng/ml; PeproTech, catalog #200-34) and granulocyte-macrophage colony stimulating factor (GM-CSF) (10 ng/ml; PeproTech, catalog #300-03) to Dulbecco's modified Eagle's medium (DMEM)/F12 (HyClone, catalog #SH30023.01) containing N-2 supplement (Gibco, catalog #17502048). This protocol facilitated the maturation process of the PMPs into microglia.

Mouse glia culture

The animal work was conducted without gender bias under the Institutional Animal Care and Use Committee (IACUC) protocol (PROTO999900242) approved by Rutgers University IACUC Committee. Primary astrocyte cultures were prepared using wild-type C57BL/6J mice aged between postnatal days 1 and 3 (P1 and P3), as reported (*86, 87*). Mouse cortices were enzymatically digested with papain in a solution containing 1 μM $Ca2^{+}$ and 0.5 μM EDTA for 15 min at 37°C. After two passages to eliminate mouse neurons, the glial cells were cultured in DMEM (Gibco, catalog #11995065) supplemented with 10% fetal bovine serum.

Generation of coculture of iPSC-iNs and iPSC-derived microglia

We utilized a mid-PRS line [line 420 (*58*)] iPSC sourced from the NIAAA/COGA Sharing Repository to generate excitatory-induced neurons (Ngn2-iNs), following the protocol as described in (*57*).In brief, when the iPSCs reached a confluency of approximately 70%, they were dissociated using Accutase and subsequently plated onto a six-well plate coated with Matrigel Matrix. These plated cells were then cultured in mTeSR plus medium, which contained RHO/ROCK pathway inhibitor Y-27632, doxycycline-inducible lentiviruses expressing transcription factors (Ngn2), and the reverse tetracycline-controlled transactivator (rtTA). The cells were cultured at 37°C with 5% CO_2. After around 6 to 8 hours of lentivirus infection, the culture medium was replaced with Neurobasal medium (Gibco, catalog #21103049). This medium was supplemented with B-27 supplement (Gibco, catalog #17504044), L-glutamine (Gibco, catalog #35050061), and doxycycline (2 mg/ml; MP Biomedicals) to induce TetO expression.

The lentivirus generation protocol was previously outlined by Wang *et al.* (*88*). Selection with puromycin (1 mg/ml; Sigma-Aldrich, catalog #P8833) was carried out for the next 2 days. On day 5, the Ngn2-iNs (approximately 200,000 iNs per coverslip) were dissociated using Accutase and plated on glass coverslips coated with primary mouse glia (approximately 50,000 cells per coverslip). On day 6, fresh Neurobasal medium containing B-27 supplement, L-glutamine, Ara-C (4 mM; Sigma-Aldrich, catalog #C6645), brain-derived neurotrophic factor (BDNF) (10 ng/ml; PeproTech, catalog #450-02), NT3 (10 ng/ml; PeproTech, catalog #450-03), and glial cell line–derived neurotrophic factor (GDNF) (10 ng/ml; PeproTech, catalog #450-10) were added. Subsequently, every 5 days, starting from day 6, 50% of the culture medium was replaced with fresh Neurobasal medium supplemented with B27, L-glutamine, BDNF, NT3, and GDNF.

On day 14, iPSC-derived microglia (approximately 30,000 cells per coverslip; table S1) were added into the Ngn2-iNs using fresh Neurobasal medium containing B-27 supplement, L-glutamine, BDNF, NT3, GDNF, IL-34, and GM-CSF. Molecular, morphological, and functional analyses were conducted approximately 5 weeks after the initial induction with doxycycline.

Intermittent ethanol exposure

Following a 7-day maturation period in DMEM/F12 medium supplemented with N2, IL-34, and GM-CSF, human-derived microglia were subjected to a 7-day chronic intermittent exposure paradigm using ethanol 200 Proof (Decon Laboratories, catalog #2716) at concentrations of 0 mM (control), 20 mM, and 75 mM, in accordance with established protocols (*89–91*). Because ethanol is depleted in culture by evaporation (*92*), we replenished half the medium daily with the 20 or 75 mM ethanol throughout the intermittent ethanol exposure period. This meticulous daily renewal of the culture medium ensured continuous intermittent ethanol exposure, enabling the investigation of the effects of ethanol on these microglia.

Immunohistochemistry

For immunocytochemistry analysis, the cultured cells were fixed using freshly prepared buffered 4% paraformaldehyde. Subsequently, after permeabilization for 10 min with 0.2% Triton X-100 in phosphate-buffered saline (PBS) and blocking with goat serum, the cell cultures underwent an antibody-labeling procedure. Specifically, the cultures were incubated overnight at 4°C with the following primary antibodies, which were diluted in blocking buffer: rabbit anti-CD235a (Thermo Fisher Scientific, catalog #PA5-27154, RRID: AB_2544630), mouse anti-CD43 (Thermo Fisher Scientific, catalog #14-0439-82, RRID: AB_763493), chicken anti-IBA1 (Aves Labs, catalog #IBA1-0020, RRID: AB_2910556), mouse anti-TMEM119 (Cell Signaling Technology, catalog #41134S, RRID: AB_3094467), rabbit anti-P2RY12 (Sigma-Aldrich, catalog #HPA014518, RRID: AB_2669027), rabbit anti-PU.1 (Cell Signaling Technology, catalog #2266S, RRID: AB_10692379), rabbit anti-CX3CR1 (Bio-Rad, catalog #AHP1589, RRID: AB_2087421), mouse anti-CD68 (Thermo Fisher Scientific, catalog #MA5-13324, RRID: AB_10987212), mouse anti-CLEC7A (R&D Systems, catalog #MAB1859, RRID: AB_2081791), and mouse anti-γH2AX (phospho-histone Ser^{139}, Millipore Sigma, catalog #05-636, RRID: AB_309864), chicken anti-MAP2 (EMD Millipore, catalog #AB5543, RRID: AB_571049), and mouse anti–synapsin 1 (Synaptic Systems, catalog #106011, RRID: AB_2619772). After incubation with primary antibodies and subsequent PBS washes, the cultures were exposed to secondary antibodies labeled with Alexa Fluor 488, 546, or 633, as appropriate (anti-mouse and/or anti-rabbit and/or anti-chicken from Thermo Fisher Scientific) for one hour at room temperature. To visualize cell nuclei, 4′,6-diamidino-2-phenylindole (DAPI, Sigma-Aldrich, catalog #F6057) was used for nuclear staining. After staining, the samples were rinsed with PBS and mounted for analysis. Microscopic images were captured using a confocal microscope (Zeiss LSM700) for further examination and data acquisition.

Image analysis

All images were acquired using Z stack maximal projection in Zeiss Zen blue software.

To analyze microglial morphology at the single-cell level, we used the "FracLac plugin" in ImageJ (https://imagej.net/ij/plugins/fraclac/FLHelp/Introduction.htm) after we collected the binary images of each microglial cell (*93*). Here, we use the parameters including fractal dimension (D), lacunarity, convex hull area (CHA), convex hull perimeter (CHP), cell circularity (CC), and convex hull span ratio to assess the complexity and circularity of microglial cells. Fractal D is the method for discerning various microglial shapes, ranging from simple round forms to intricate branched structures (*94, 95*). In this study, box-counting software was used to enumerate the number of boxes encompassing any foreground pixels within the outlined images, which were progressively processed on grids of diminishing calibers. Lacunarity indicates variations in the soma and additional morphological features. This parameter quantifies shape heterogeneity, both in terms of translation and rotation invariance (*95*). Lacunarity is computed using the box-counting software FracLac, representing the pixel mass distribution in microglia images. CHP is the single outline of the convex hull expressed in microns. CHA refers to the measurement of the area enclosed by the smallest convex polygon, which is defined as a polygon with all interior angles smaller than 180 degrees, encompassing the entire cell shape. CC was calculated as $(4\pi \times \text{cell area})/(\text{cell perimeter})^2$. The circularity value of a circle is 1. The convex hull span ratio is determined by calculating the ratio between the major and minor axes of the convex hull.

The analysis of synaptic puncta density was performed on iNs at day 35. This analysis was conducted using the dendrite marker MAP2 and synaptic markers synapsin 1. The quantification of correlated synaptic puncta size and intensity was performed using Intellicount (*62*).

RNA library construction, quality control, and sequencing

Total RNA from iPSC and iPSC-derived microglia was extracted using RNeasy Plus kit (QIAGEN, catalog #74136). Library construction and sequencing were performed by Novogene. The mRNA was purified from total RNA using poly-T oligo-attached magnetic beads. After fragmentation, the first strand cDNA was synthesized using random hexamer primers, followed by the second strand cDNA synthesis using either deoxyuridine triphosphate nick end labeling for a directional library or 3′-deoxythymidine 5′-triphosphate for the nondirectional library. The nondirectional library was ready after end repair, A-tailing, adapter ligation, size selection, amplification, and purification. The library was prepared through end repair, A-tailing, adapter ligation, size selection, USER enzyme digestion, amplification, and purification steps. The library was checked with Qubit and real-time polymerase chain reaction for quantification and bioanalyzer for size distribution detection. Quantified libraries were pooled and sequenced on Illumina NextSeq500 platforms by Novogene. Approximately 40 to 60 million paired reads were generated for each sample (table S3). Reads were aligned to the hg38 human reference genome by HISAT2 (v.2.1.0) (*96*). Transcript counts were extracted using the featureCounts function of the Rsubread package. Details of the bioinformatics analysis methods for RNA-seq data are provided in the Supplementary Materials.

Analyses of genomic integrity using e-karyotyping analysis and G-band karyotyping analysis

The genomic integrity of all iPSC lines was assessed using eSNP-karyotyping analysis. The eSNP-karyotyping was conducted as previously described (*44*). Briefly, SNPs were identified using GATK HaplotypeCaller and then filtered by read depth and allelic frequency to minimize errors. SNPs with low coverage (under 20 reads) or minor allele frequency below 0.2 were excluded. For each SNP, the major-to-minor frequency ratio was computed and organized by chromosomal position. Visualization involved plotting moving medians of these ratios along chromosomal positions. Statistical significance was determined with a one-tailed *t* test, adjusted for multiple testing using false discovery rate. G-band karyotyping analysis of the selected iPSCs was conducted by Cell Line Genetics (https://clgenetics.com/our-services/g-band-karyotyping/).

Synaptosomes extraction and pHrodo red conjugation

Synaptosomes were extracted from iPSC-derived iNs at day 40 using Syn-PER synaptic protein extraction reagent (Thermo Fisher Scientific, catalog #87793) and conjugated with pHrodo red amine-reactive labels (Life Technologies, catalog #P36600) following the manufacturer's instructions. Syn-PER reagent (400 μl for one well in six-well plates) was added to iNs. Cells were scraped to collect lysate and then centrifuged at 1200*g* for 10 min at 4°C. The supernatant was transferred to a new tube and centrifuged at 15,000*g* for 20 min at 4°C to retain the synaptosome pellet. The synaptosome pellet (200 μg) was suspended in 100 μl of 0.1 M $NaHCO_3$ (pH 8.3) and 1 μl of pHrodo red dye. The suspension was then incubated on a twist shaker at 40 rpm for 1.5 hours at room temperature, covered with aluminum foil. After incubation, ice-cold Dulbecco's PBS (DPBS) was added, followed by centrifugation at 13,000 rpm for 2 min at 4°C. The pellet was washed five times with DPBS to remove unbound dye. Last, the pellet was resuspended in 100 μl of DPBS with 5% dimethyl sulfoxide.

Phagocytosis assay

In the phagocytosis assay, human iPSC-derived microglia were seeded in a 96-well plate following a 7-day intermittent ethanol exposure paradigm at varying concentrations (0 mM as the control, 20 mM, and 75 mM for phagocytosis of beads, and 0 mM and 75 mM for phagocytosis of synaptosomes). On day 7 of ethanol exposure, minocycline hydrochloride (60 μM; Sigma-Aldrich, CAS:13614-98-7) and cytochalasin D (2 μM; Thermo Fisher Scientific, catalog #PHZ1063) were added 24 hours before conducting the phagocytosis assay. To visualize the cell nuclei, Hoechst stain was diluted at a ratio of 1:1000 and added to the microglia, followed by incubation at 37°C for 10 min. Zymosan bioparticles (Thermo Fisher Scientific, catalog #P35364) or synaptosomes linked with pHrodo red dye were prepared by vortexing and then subjected to ultrasonication for 5 min. These zymosan bioparticles or synaptosomes were then added to the live microglia in the live-cell imaging solution (Thermo Fisher Scientific, catalog #A14291DJ), and the cells were incubated for 2 hours at 37°C. Live-cell images were acquired using a BZ-x800 microscope equipped with Keyence BZ-x800 software for subsequent analysis and data collection.

Western blot

Synaptosomes were lysed using radioimmunoprecipitation assay (RIPA) buffer [50 mM tris-HCl, 150 mM NaCl, 1% NP-40 (IGEPAL® CA-630, Sigma-Aldrich, catalog #I8896), 0.5% sodium deoxycholate,

0.14 SDS, 1 mM dithiothreitol, and 1X protease inhibitor cocktail] to isolate synaptic proteins. The isolated synaptic protein was quantified using the Pierce BCA Protein Assay Kit (Thermo Fisher Scientific, catalog #23225). Dissociated mouse brains and induced neuronal cultures served as controls and subjected to a similar protocol of protein extraction and lysis using RIPA buffer.

The proteins were then diluted with 2X SDS loading buffer [4% SDS, 125 mM (pH 6.8) tris-HCl, 20% glycerol, 5% 2-mercaptoethanol, and 0.01% bromophenol blue] and denatured by heating to 95°C for 5 min. After cooling, the denatured protein samples were loaded into separate wells of 10% TGX gels (Bio-Rad, catalog #4561033 DC) along with a precision plus protein (10 to 250 kDa) dual color standards (Bio-Rad, catalog #1610374) ladder. Western blots were run for 2 hours at 80 volts and 400 mA. Proteins from the gel were transferred to a 0.45-μm nitrocellulose membrane (Bio-Rad, catalog #1620115) using the Bio-Rad transferring system for 2 hours at a constant 100 V at 4°C. The nitrocellulose membrane was blocked in 5% nonfat milk for 1 hour at room temperature and then incubated with primary antibodies (1:1000; synapsin 1, Synaptic Systems, RRID: AB_2619772; synaptotagmin 1, Santa Cruz Biotechnology, catalog #sc-136480; PSD95, Synaptic systems, catalog #124011; syntaxin, I378, custom made, gift of T. Südhof) overnight at 4°C. The following day, the blots were washed three times with tris-buffered saline with 0.1% Tween 20 (TBST) before incubating with horseradish peroxidase–conjugated secondary antibody (1:5000) at room temperature for 1 hour. After four washes with TBST, the blots were incubated with clarity Western ECL substrate (Bio-Rad, catalog #1705060) for 1 min before developing the membrane on autoradiographic films (Lab Scientific, catalog #XAR ALF 1318).

Electrophysiology

Functional analyses of iN cells were conducted using whole-cell patch-clamp electrophysiology as described elsewhere (*88, 97*). Miniature postsynaptic currents were recorded at a holding potential of −70 mV in the presence of 1 μM tetrodotoxin. Cs-based solution was used, which consisted of 40 mM CsCl, 3.5 mM KCl, 10 mM Hepes, 0.05 mM EGTA, 90 mM K-gluconate, 1.8 mM NaCl, 1.7 mM $MgCl_2$, 2 mM adenosine 5′-triphosphate (ATP)–magnesium, 0.4 mM guanosine 5′-triphosphate–sodium, and 10 mM phosphocreatine. The recording batch solution contained 140 mM NaCl, 5 mM KCl, 10 mM Hepes, 2 mM $CaCl_2$, 2 mM $MgCl_2$, and 10 mM glucose (pH 7.4). All cell culture recordings were conducted at room temperature.

Statistical analysis

Statistical analyses were performed using GraphPad Prism version 10.0 (GraphPad Software, La Jolla, CA). Data are presented as the means ± SEM, unless stated otherwise. Statistical analysis was performed on data derived from biologically independent experimental replicates, as specified in the figure legends. The impact of chronic ethanol application was assessed by normalizing the results to the baseline activity in high-PRS microglia, with changes in high-PRS and low-PRS microglia relative to baseline values defined as relative changes. Differences in the effects of various ethanol concentrations in high-PRS and low-PRS microglia were evaluated using a two-way analysis of variance (ANOVA), followed by post hoc analysis with Fisher's least significant difference test for multiple comparisons. Within the same group of microglia, the effects of ethanol before and after application were compared using unpaired *t* tests. Statistical significance was indicated by the following symbols: ($^*P < 0.05$, $^{**}P < 0.01$, and $^{***}P < 0.001$), with (NS) denoting no statistically significant difference.

Supplementary Materials

This PDF file includes:

Supplementary Text
Figs. S1 to S8
Tables S1 to S3
References

REFERENCES AND NOTES

1. A. F. Carvalho, M. Heilig, A. Perez, C. Probst, J. Rehm, Alcohol use disorders. *Lancet* **394**, 781–792 (2019).
2. B. Verhulst, M. C. Neale, K. S. Kendler, The heritability of alcohol use disorders: A meta-analysis of twin and adoption studies. *Psychol. Med.* **45**, 1061–1072 (2015).
3. G. R. B. Saunders, X. Wang, F. Chen, S.-K. Jang, M. Liu, C. Wang, S. Gao, Y. Jiang, C. Khunsriraksakul, J. M. Otto, C. Addison, M. Akiyama, C. M. Albert, F. Aliev, A. Alonso, D. K. Arnett, A. E. Ashley-Koch, A. A. Ashrani, K. C. Barnes, R. G. Barr, T. M. Bartz, D. M. Becker, L. F. Bielak, E. J. Benjamin, J. C. Bis, G. Bjornsdottir, J. Blangero, E. R. Bleecker, J. D. Boardman, E. Boerwinkle, D. I. Boomsma, M. P. Boorgula, D. W. Bowden, J. A. Brody, B. E. Cade, D. I. Chasman, S. Chavan, Y.-D. I. Chen, Z. Chen, I. Cheng, M. H. Cho, H. Choquet, J. W. Cole, M. C. Cornelis, F. Cucca, J. E. Curran, M. de Andrade, D. M. Dick, A. R. Docherty, R. Duggirala, C. B. Eaton, M. A. Ehringer, T. Esko, J. D. Faul, L. F. Silva, E. Fiorillo, M. Fornage, B. I. Freedman, M. E. Gabrielsen, M. E. Garrett, S. A. Gharib, C. Gieger, N. Gillespie, D. C. Glahn, S. D. Gordon, C. C. Gu, D. Gu, D. F. Gudbjartsson, X. Guo, J. Haessler, M. E. Hall, T. Haller, K. M. Harris, J. He, P. Herd, J. K. Hewitt, I. Hickie, B. Hidalgo, J. E. Hokanson, C. Hopfer, J. J. Hottenga, L. Hou, H. Huang, Y.-J. Hung, D. J. Hunter, K. Hveem, S.-J. Hwang, C.-M. Hwu, W. Iacono, M. R. Irvin, Y. H. Jee, E. O. Johnson, Y. Y. Joo, E. Jorgenson, A. E. Justice, Y. Kamatani, R. C. Kaplan, J. Kaprio, S. L. R. Kardia, M. C. Keller, T. N. Kelly, C. Kooperberg, T. Korhonen, P. Kraft, K. Krauter, J. Kuusisto, M. Laakso, J. Lasky-Su, W.-J. Lee, J. J. Lee, D. Levy, L. Li, K. Li, Y. Li, K. Lin, P. A. Lind, C. Liu, D. M. Lloyd-Jones, S. M. Lutz, J. Ma, R. Mägi, A. Manichaikul, N. G. Martin, R. Mathur, N. Matoba, P. F. Mc Ardle, M. M. Gue, M. B. Mc Queen, S. E. Medland, A. Metspalu, D. A. Meyers, I. Y. Millwood, B. D. Mitchell, K. L. Mohlke, M. Moll, M. E. Montasser, A. C. Morrison, A. Mulas, J. B. Nielsen, K. E. North, E. C. Oelsner, Y. Okada, V. Orrù, N. D. Palmer, T. Palviainen, A. Pandit, S. L. Park, U. Peters, A. Peters, P. A. Peyser, T. J. C. Polderman, N. Rafaels, S. Redline, R. M. Reed, A. P. Reiner, J. P. Rice, S. S. Rich, N. E. Richmond, C. Roan, J. I. Rotter, M. N. Rueschman, V. Runarsdottir, N. L. Saccone, D. A. Schwartz, A. H. Shadyab, J. Shi, S. S. Shringarpure, K. Sicinski, A. H. Skogholt, J. A. Smith, N. L. Smith, N. Sotoodehnia, M. C. Stallings, H. Stefansson, K. Stefansson, J. A. Stitzel, X. Sun, M. Syed, R. Tal-Singer, A. E. Taylor, K. D. Taylor, M. J. Telen, K. K. Thai, H. Tiwari, C. Turman, T. Tyrfingsson, T. L. Wall, R. G. Walters, D. R. Weir, S. T. Weiss, W. B. White, J. B. Whitfield, K. L. Wiggins, G. Willemsen, C. J. Willer, B. S. Winsvold, H. Xu, L. R. Yanek, J. Yin, K. L. Young, K. A. Young, B. Yu, W. Zhao, W. Zhou, S. Zöllner, L. Zuccolo; 23andMe Research Team; The Biobank Japan Project, C. Batini, A. W. Bergen, L. J. Bierut, S. P. David, S. A. Gagliano Taliun, D. B. Hancock, B. Jiang, M. R. Munafò, T. E. Thorgeirsson, D. J. Liu, S. Vrieze, Genetic diversity fuels gene discovery for tobacco and alcohol use. *Nature* **612**, 720–724 (2022).
4. J. Su, S. I. Kuo, F. Aliev, J. A. Rabinowitz, B. Jamil, G. Chan, H. J. Edenberg, M. Francis, V. Hesselbrock, C. Kamarajan, S. Kinreich, J. Kramer, D. Lai, V. McCutcheon, J. Meyers, A. Pandey, G. Pandey, M. H. Plawecki, M. Schuckit, J. Tischfield, D. M. Dick, Alcohol use polygenic risk score, social support, and alcohol use among European American and African American adults, in *Development and Psychopathology* (Cambridge Univ. Press, (2023), pp. 1–13.
5. J. D. Deak, E. C. Johnson, Genetics of substance use disorders: A review. *Psychol. Med.* **51**, 2189–2200 (2021).
6. H. R. Kranzler, H. Zhou, R. L. Kember, R. Vickers Smith, A. C. Justice, S. Damrauer, P. S. Tsao, D. Klarin, A. Baras, J. Reid, J. Overton, D. J. Rader, Z. Cheng, J. P. Tate, W. C. Becker, J. Concato, K. Xu, R. Polimanti, H. Zhao, J. Gelernter, Genome-wide association study of alcohol consumption and use disorder in 274,424 individuals from multiple populations. *Nat. Commun.* **10**, 1499 (2019).
7. A. B. Hart, H. R. Kranzler, Alcohol dependence genetics: lessons learned from genome-wide association studies (GWAS) and post-GWAS analyses. *Alcohol Clin. Exp. Res.* **39**, 1312–1327 (2015).
8. N. R. Wray, S. H. Lee, D. Mehta, A. A. Vinkhuyzen, F. Dudbridge, C. M. Middeldorp, Research review: Polygenic methods and their application to psychiatric traits. *J. Child. Psychol. Psychiatry* **55**, 1068–1087 (2014).
9. G. Ni, J. Zeng, J. A. Revez, Y. Wang, Z. Zheng, T. Ge, R. Restuadi, J. Kiewa, D. R. Nyholt, J. R. I. Coleman, J. W. Smoller, J. Yang, P. M. Visscher, N. R. Wray, A comparison of ten polygenic score methods for psychiatric disorders applied across multiple cohorts. *Biol. Psychiatry* **90**, 611–620 (2021).
10. D. Lai, E. C. Johnson, S. Colbert, G. Pandey, G. Chan, L. Bauer, M. W. Francis, V. Hesselbrock, C. Kamarajan, J. Kramer, W. Kuang, S. Kuo, S. Kuperman, Y. Liu, V. McCutcheon, Z. Pang, M. H. Plawecki, M. Schuckit, J. Tischfield, L. Wetherill, Y. Zang, H. J. Edenberg, B. Porjesz, A. Agrawal, T. Foroud, Evaluating risk for alcohol use disorder: Polygenic risk scores and family history. *Alcohol Clin. Exp. Res.* **46**, 374–383 (2022).

11. J. E. Savage, J. E. Salvatore, F. Aliev, A. C. Edwards, M. Hickman, K. S. Kendler, J. Macleod, A. Latvala, A. Loukola, J. Kaprio, R. J. Rose, G. Chan, V. Hesselbrock, B. T. Webb, A. Adkins, T. B. Bigdeli, B. P. Riley, D. M. Dick, Polygenic risk score prediction of alcohol dependence symptoms across population-based and clinically ascertained samples. *Alcohol Clin. Exp. Res.* **42**, 520–530 (2018).
12. P. B. Barr, A. Ksinan, J. Su, E. C. Johnson, J. L. Meyers, L. Wetherill, A. Latvala, F. Aliev, G. Chan, S. Kuperman, J. Nurnberger, C. Kamarajan, A. Anokhin, A. Agrawal, R. J. Rose, H. J. Edenberg, M. Schuckit, J. Kaprio, D. M. Dick, Using polygenic scores for identifying individuals at increased risk of substance use disorders in clinical and population samples. *Transl. Psychiatry* **10**, 196 (2020).
13. E. K. Erickson, E. K. Grantham, A. S. Warden, R. A. Harris, Neuroimmune signaling in alcohol use disorder. *Pharmacol. Biochem. Behav.* **177**, 34–60 (2019).
14. M. Kapoor, J. C. Wang, S. P. Farris, Y. Liu, J. McClintick, I. Gupta, J. L. Meyers, S. Bertelsen, M. Chao, J. Nurnberger, J. Tischfield, O. Harari, L. Zeran, V. Hesselbrock, L. Bauer, T. Raj, B. Porjesz, A. Agrawal, T. Foroud, H. J. Edenberg, R. D. Mayfield, A. Goate, Analysis of whole genome-transcriptomic organization in brain to identify genes associated with alcoholism. *Transl. Psychiatry* **9**, 89 (2019).
15. L. De Filippis, A. Halikere, H. McGowan, J. C. Moore, J. A. Tischfield, R. P. Hart, Z. P. Pang, Ethanol-mediated activation of the NLRP3 inflammasome in iPS cells and iPS cells-derived neural progenitor cells. *Mol. Brain* **9**, 51 (2016).
16. V. H. Perry, A revised view of the central nervous system microenvironment and major histocompatibility complex class II antigen presentation. *J. Neuroimmunol.* **90**, 113–121 (1998).
17. D. Gosselin, D. Skola, N. G. Coufal, I. R. Holtman, J. C. M. Schlachetzki, E. Sajti, B. N. Jaeger, C. O'Connor, C. Fitzpatrick, M. P. Pasillas, M. Pena, A. Adair, D. D. Gonda, M. L. Levy, R. M. Ransohoff, F. H. Gage, C. K. Glass, An environment-dependent transcriptional network specifies human microglia identity. *Science* **356**, eaal3222 (2017).
18. T. R. Hammond, C. Dufort, L. Dissing-Olesen, S. Giera, A. Young, A. Wysoker, A. J. Walker, F. Gergits, M. Segel, J. Nemesh, S. E. Marsh, A. Saunders, E. Macosko, F. Ginhoux, J. Chen, R. J. M. Franklin, X. Piao, S. A. McCarroll, B. Stevens, Single-cell RNA sequencing of microglia throughout the mouse lifespan and in the injured brain reveals complex cell-state changes. *Immunity* **50**, 253–271.e6 (2019).
19. T. Matsudaira, M. Prinz, Life and death of microglia: Mechanisms governing microglial states and fates. *Immunol. Lett.* **245**, 51–60 (2022).
20. Y. Liu, X. Shen, Y. Zhang, X. Zheng, C. Cepeda, Y. Wang, S. Duan, X. Tong, Interactions of glial cells with neuronal synapses, from astrocytes to microglia and oligodendrocyte lineage cells. *Glia* **71**, 1383–1401 (2023).
21. D. P. Schafer, E. K. Lehrman, A. G. Kautzman, R. Koyama, A. R. Mardinly, R. Yamasaki, R. M. Ransohoff, M. E. Greenberg, B. A. Barres, B. Stevens, Microglia sculpt postnatal neural circuits in an activity and complement-dependent manner. *Neuron* **74**, 691–705 (2012).
22. S. A. Marshall, C. R. Geil, K. Nixon, Prior binge ethanol exposure potentiates the microglial response in a model of alcohol-induced neurodegeneration. *Brain Sci.* **6**, 16 (2016).
23. S. A. Marshall, J. A. McClain, M. L. Kelso, D. M. Hopkins, J. R. Pauly, K. Nixon, Microglial activation is not equivalent to neuroinflammation in alcohol-induced neurodegeneration: The importance of microglia phenotype. *Neurobiol. Dis.* **54**, 239–251 (2013).
24. S. Mukherjee, M. A. Cabrera, N. I. Boyadjieva, G. Berger, B. Rousseau, D. K. Sarkar, Alcohol increases exosome release from microglia to promote complement C1q-induced cellular death of proopiomelanocortin neurons in the hypothalamus in a rat model of fetal alcohol spectrum disorders. *J. Neurosci.* **40**, 7965–7979 (2020).
25. L. G. Chastain, D. K. Sarkar, Role of microglia in regulation of ethanol neurotoxic action. *Int. Rev. Neurobiol.* **118**, 81–103 (2014).
26. T. J. Walter, F. T. Crews, Microglial depletion alters the brain neuroimmune response to acute binge ethanol withdrawal. *J. Neuroinflammation* **14**, 86 (2017).
27. A. S. Warden, S. A. Wolfe, S. Khom, F. P. Varodayan, R. R. Patel, M. Q. Steinman, M. Bajo, S. E. Montgomery, R. Vlkolinsky, T. Nadav, I. Polis, A. J. Roberts, R. D. Mayfield, R. A. Harris, M. Roberto, Microglia control escalation of drinking in alcohol-dependent mice: Genomic and synaptic drivers. *Biol. Psychiatry* **88**, 910–921 (2020).
28. L. Lan, H. Wang, X. Zhang, Q. Shen, X. Li, L. He, X. Rong, J. Peng, J. Mo, Y. Peng, Chronic exposure of alcohol triggers microglia-mediated synaptic elimination inducing cognitive impairment. *Exp. Neurol.* **353**, 114061 (2022).
29. T. F. Galatro, I. R. Holtman, A. M. Lerario, I. D. Vainchtein, N. Brouwer, P. R. Sola, M. M. Veras, T. F. Pereira, R. E. P. Leite, T. Möller, P. D. Wes, M. C. Sogayar, J. D. Laman, W. den Dunnen, C. A. Pasqualucci, S. M. Oba-Shinjo, E. Boddeke, S. K. N. Marie, B. J. L. Eggen, Transcriptomic analysis of purified human cortical microglia reveals age-associated changes. *Nat. Neurosci.* **20**, 1162–1171 (2017).
30. R. Xu, X. Li, A. J. Boreland, A. Posyton, K. Kwan, R. P. Hart, P. Jiang, Human iPSC-derived mature microglia retain their identity and functionally integrate in the chimeric mouse brain. *Nat. Commun.* **11**, 1577 (2020).
31. E. M. Abud, R. N. Ramirez, E. S. Martinez, L. M. Healy, C. H. H. Nguyen, S. A. Newman, A. V. Yeromin, V. M. Scarfone, S. E. Marsh, C. Fimbres, C. A. Caraway, G. M. Fote, A. M. Madany, A. Agrawal, R. Kayed, K. H. Gylys, M. D. Cahalan, B. J. Cummings, J. P. Antel, A. Mortazavi, M. J. Carson, W. W. Poon, M., Blurton-Jones, iPSC-derived human microglia-like cells to study neurological diseases. *Neuron* **94**, 278–293.e9 (2017).
32. R. Xu, A. J. Boreland, X. Li, C. Erickson, M. Jin, C. Atkins, Z. Pang, B. P. Daniels, P. Jiang, Developing human pluripotent stem cell-based cerebral organoids with a controllable microglia ratio for modeling brain development and pathology. *Stem Cell Rep.* **16**, 1923–1937 (2020).
33. S. R. Guttikonda, L. Sikkema, J. Tchieu, N. Saurat, R. M. Walsh, O. Harschnitz, G. Ciceri, M. Sneeboer, L. Mazutis, M. Setty, P. Zumbo, D. Betel, L. D. de Witte, D. Pe'er, L. Studer, Fully defined human pluripotent stem cell-derived microglia and tri-culture system model C3 production in Alzheimer's disease. *Nat. Neurosci.* **24**, 343–354 (2021).
34. M. Jin, Z. Ma, P. Jiang, Generation of iPSC-based human-mouse microglial brain chimeras to study senescence of human microglia. *STAR Protoc.* **3**, 101847 (2022).
35. D. S. Svoboda, M. I. Barrasa, J. Shu, R. Rietjens, S. Zhang, M. Mitalipova, P. Berube, D. Fu, L. D. Shultz, G. W. Bell, R. Jaenisch, Human iPSC-derived microglia assume a primary microglia-like state after transplantation into the neonatal mouse brain. *Proc. Natl. Acad. Sci. U.S.A.* **116**, 25293–25303 (2019).
36. A. J. Boreland, A. C. Stillitano, H. C. Lin, Y. Abbo, R. P. Hart, P. Jiang, Z. P. Pang, A. B. Rabson, Dysregulated neuroimmune interactions and sustained type I interferon signaling after human immunodeficiency virus type 1 infection of human iPSC derived microglia and cerebral organoids. bioRxiv 563950 [Preprint] (2023).
37. M. J. Dolan, M. Therrien, S. Jereb, T. Kamath, V. Gazestani, T. Atkeson, S. E. Marsh, A. Goeva, N. M. Lojek, S. Murphy, C. M. White, J. Joung, B. Liu, F. Limone, K. Eggan, N. Hacohen, B. E. Bernstein, C. K. Glass, V. Leinonen, M. Blurton-Jones, F. Zhang, C. B. Epstein, E. Z. Macosko, B. Stevens, Exposure of iPSC-derived human microglia to brain substrates enables the generation and manipulation of diverse transcriptional states in vitro. *Nat. Immunol.* **24**, 1382–1390 (2023).
38. J. F. Henriques, C. C. Portugal, T. Canedo, J. B. Relvas, T. Summavielle, R. Socodato, Microglia and alcohol meet at the crossroads: Microglia as critical modulators of alcohol neurotoxicity. *Toxicol. Lett.* **283**, 21–31 (2018).
39. E. K. Erickson, Y. A. Blednov, R. A. Harris, R. D. Mayfield, Glial gene networks associated with alcohol dependence. *Sci. Rep.* **9**, 10949 (2019).
40. J. He, F. T. Crews, Increased MCP-1 and microglia in various regions of the human alcoholic brain. *Exp. Neurol.* **210**, 349–358 (2008).
41. E. C. Johnson, J. E. Salvatore, D. Lai, A. K. Merikangas, J. I. Nurnberger, J. A. Tischfield, X. Xuei, C. Kamarajan, L. Wetherill, J. P. Rice, J. R. Kramer, S. Kuperman, T. Foroud, P. A. Slesinger, A. M. Goate, B. Porjesz, D. M. Dick, H. J. Edenberg, A. Agrawal, The collaborative study on the genetics of alcoholism: Genetics. *Genes Brain Behav.* **22**, e12856 (2023).
42. A. Agrawal, S. J. Brislin, K. K. Bucholz, D. Dick, R. P. Hart, E. C. Johnson, J. Meyers, J. Salvatore, P. Slesinger; COGA Collaborators, L. Almasy, T. Foroud, A. Goate, V. Hesselbrock, J. Kramer, S. Kuperman, A. K. Merikangas, J. I. Nurnberger, J. Tischfield, H. J. Edenberg, B. Porjesz, The collaborative study on the genetics of alcoholism: Overview. *Genes Brain Behav.* **22**, e12864 (2023).
43. I. Gameiro-Ros, D. Popova, I. Prytkova, Z. P. Pang, Y. Liu, D. Dick, K. K. Bucholz, A. Agrawal, B. Porjesz, A. M. Goate, X. Xuei, C. Kamarajan; COGA Collaborators, J. A. Tischfield, H. J. Edenberg, P. A. Slesinger, R. P. Hart, 5. Collaborative study on the genetics of alcoholism: Functional genomics. *Genes Brain Behav.* **22**, e12855 (2023).
44. U. Weissbein, M. Schachter, D. Egli, N. Benvenisty, Analysis of chromosomal aberrations and recombination by allelic bias in RNA-seq. *Nat. Commun.* **7**, 12144 (2016).
45. H. Mathys, Z. Peng, C. A. Boix, M. B. Victor, N. Leary, S. Babu, G. Abdelhady, X. Jiang, A. P. Ng, K. Ghafari, A. K. Kunisky, J. Mantero, K. Galani, V. N. Lohia, G. E. Fortier, Y. Lotfi, J. Ivey, H. P. Brown, P. R. Patel, N. Chakraborty, J. I. Beaudway, E. J. Imhoff, C. F. Keeler, M. M. McChesney, H. H. Patel, S. P. Patel, M. T. Thai, D. A. Bennett, M. Kellis, L. H. Tsai, Single-cell atlas reveals correlates of high cognitive function, dementia, and resilience to Alzheimer's disease pathology. *Cell* **186**, 4365–4385.e27 (2023).
46. M. S. Scarnati, A. Halikere, Z. P. Pang, Using human stem cells as a model system to understand the neural mechanisms of alcohol use disorders: Current status and outlook. *Alcohol* **74**, 83–93 (2019).
47. J. Cornell, S. Salinas, H. Y. Huang, M. Zhou, Microglia regulation of synaptic plasticity and learning and memory. *Neural Regen. Res.* **17**, 705–716 (2022).
48. Q. Li, D. Liu, F. Pan, C. S. H. Ho, R. C. M. Ho, Ethanol exposure induces microglia activation and neuroinflammation through TLR4 activation and SENP6 modulation in the adolescent rat hippocampus. *Neural Plast.* **2019**, 1648736 (2019).
49. A. M. Jurga, M. Paleczna, K. Z. Kuter, Overview of general and discriminating markers of differential microglia phenotypes. *Front. Cell Neurosci.* **14**, 198 (2020).
50. M. Prinz, S. Jung, J. Priller, Microglia biology: One century of evolving concepts. *Cell* **179**, 292–311 (2019).
51. H. J. Edenberg, J. N. McClintick, alcohol dehydrogenases, aldehyde dehydrogenases, and alcohol use disorders: A critical review. *Alcohol Clin. Exp. Res.* **42**, 2281–2297 (2018).
52. M. E. Deerhake, M. L. Shinohara, Emerging roles of Dectin-1 in noninfectious settings and in the CNS. *Trends Immunol.* **42**, 891–903 (2021).

53. L. J. Mah, A. El-Osta, T. C. Karagiannis, γH2AX: A sensitive molecular marker of DNA damage and repair. *Leukemia* **24**, 679–686 (2010).
54. J. K. Sun, D. Wu, G. C. Wong, T. M. Lau, M. Yang, R. P. Hart, K. M. Kwan, H. Y. E. Chan, H. M. Chow, Chronic alcohol metabolism results in DNA repair infidelity and cell cycle-induced senescence in neurons. *Aging Cell* **22**, e13772 (2023).
55. S. Bang, C. R. Donnelly, X. Luo, M. Toro-Moreno, X. Tao, Z. Wang, S. Chandra, A. V. Bortsov, E. R. Derbyshire, R. R. Ji, Activation of GPR37 in macrophages confers protection against infection-induced sepsis and pain-like behaviour in mice. *Nat. Commun.* **12**, 1704 (2021).
56. E. Layman, J. M. Parrott, H. Y. Lee, Protocol for assessing phagocytosis activity in cultured primary murine microglia. *STAR Protoc.* **3**, 101881 (2022).
57. Y. Zhang, C. Pak, Y. Han, H. Ahlenius, Z. Zhang, S. Chanda, S. Marro, C. Patzke, C. Acuna, J. Covy, W. Xu, N. Yang, T. Danko, L. Chen, M. Wernig, T. C. Südhof, Rapid single-step induction of functional neurons from human pluripotent stem cells. *Neuron* **78**, 785–798 (2013).
58. D. Popova, I. Gameiro-Ros, M. M. Youssef, P. Zalamea, A. D. Morris, I. Prytkova, A. Jadali, K. Y. Kwan, C. Kamarajan, J. E. Salvatore, X. Xuei, D. B. Chorlian, B. Porjesz, S. Kuperman, D. M. Dick, A. Goate, H. J. Edenberg, J. A. Tischfield, Z. P. Pang, P. A. Slesinger, R. P. Hart, Alcohol reverses the effects of KCNJ6 (GIRK2) noncoding variants on excitability of human glutamatergic neurons. *Mol. Psychiatry* **28**, 746–758 (2023).
59. T. Vierbuchen, A. Ostermeier, Z. P. Pang, Y. Kokubu, T. C. Sudhof, M. Wernig, Direct conversion of fibroblasts to functional neurons by defined factors. *Nature* **463**, 1035–1041 (2010).
60. Z. P. Pang, N. Yang, T. Vierbuchen, A. Ostermeier, D. R. Fuentes, T. Q. Yang, A. Citri, V. Sebastiano, S. Marro, T. C. Südhof, M. Wernig, Induction of human neuronal cells by defined transcription factors. *Nature* **476**, 220–223 (2011).
61. L. J. Lawson, V. H. Perry, P. Dri, S. Gordon, Heterogeneity in the distribution and morphology of microglia in the normal adult mouse brain. *Neuroscience* **39**, 151–170 (1990).
62. J. A. Fantuzzo, V. R. Mirabella, A. H. Hamod, R. P. Hart, J. D. Zahn, Z. P. Pang, *Intellicount*: High-throughput quantification of fluorescent synaptic protein puncta by machine learning. *eNeuro* **4**, ENEURO.0219-17.2017 (2017).
63. D. H. Geschwind, J. Flint, Genetics and genomics of psychiatric disease. *Science* **349**, 1489–1494 (2015).
64. P. M. Visscher, N. R. Wray, Q. Zhang, P. Sklar, M. I. McCarthy, M. A. Brown, J. Yang, 10 Years of GWAS discovery: Biology, function, and translation. *Am. J. Hum. Genet.* **101**, 5–22 (2017).
65. D. Lvovs, O. O. Favorova, A. V. Favorov, A polygenic approach to the study of polygenic diseases. *Acta Naturae* **4**, 59–71 (2012).
66. A. Nimmerjahn, F. Kirchhoff, F. Helmchen, Resting microglial cells are highly dynamic surveillants of brain parenchyma in vivo. *Science* **308**, 1314–1318 (2005).
67. H. Kettenmann, U. K. Hanisch, M. Noda, A. Verkhratsky, Physiology of microglia. *Physiol. Rev.* **91**, 461–553 (2011).
68. M. Colonna, O. Butovsky, Microglia function in the central nervous system during health and neurodegeneration. *Annu. Rev. Immunol.* **35**, 441–468 (2017).
69. A. R. Mantegazza, J. G. Magalhaes, S. Amigorena, M. S. Marks, Presentation of phagocytosed antigens by MHC class I and II. *Traffic* **14**, 135–152 (2013).
70. V. Maneu, A. Yáñez, C. Murciano, A. Molina, M. L. Gil, D. Gozalbo, Dectin-1 mediates in vitro phagocytosis of Candida albicans yeast cells by retinal microglia. *FEMS Immunol. Med. Microbiol.* **63**, 148–150 (2011).
71. A. Pellon, A. Ramirez-Garcia, X. Guruceaga, A. Zabala, I. Buldain, A. Antoran, J. Anguita, A. Rementeria, C. Matute, F. L. Hernando, Microglial immune response is impaired against the neurotropic fungus Lomentospora prolificans. *Cell Microbiol.* **20**, e12847 (2018).
72. H. Keren-Shaul, A. Spinrad, A. Weiner, O. Matcovitch-Natan, R. Dvir-Szternfeld, T. K. Ulland, E. David, K. Baruch, D. Lara-Astaiso, B. Toth, S. Itzkovitz, M. Colonna, M. Schwartz, I. Amit, A unique microglia type associated with restricting development of alzheimer's disease. *Cell* **169**, 1276–1290.e17 (2017).
73. Y. Wang, X. Zhang, Q. Song, Y. Hou, J. Liu, Y. Sun, P. Wang, Characterization of the chromatin accessibility in an Alzheimer's disease (AD) mouse model. *Alzheimers Res. Ther.* **12**, 29 (2020).
74. J. V. Haure-Mirande, M. Wang, M. Audrain, T. Fanutza, S. H. Kim, S. Heja, B. Readhead, J. T. Dudley, R. D. Blitzer, E. E. Schadt, B. Zhang, S. Gandy, M. E. Ehrlich, Correction: Integrative approach to sporadic Alzheimer's disease: Deficiency of TYROBP in cerebral Aβ amyloidosis mouse normalizes clinical phenotype and complement subnetwork molecular pathology without reducing Aβ burden. *Mol. Psychiatry* **24**, 472 (2019).
75. H. S. Yang, K. D. Onos, K. Choi, K. J. Keezer, D. A. Skelly, G. W. Carter, G. R. Howell, Natural genetic variation determines microglia heterogeneity in wild-derived mouse models of Alzheimer's disease. *Cell Rep.* **34**, 108739 (2021).
76. U. Eyo, A. V. Molofsky, Defining microglial-synapse interactions. *Science* **381**, 1155–1156 (2023).
77. T. K. Lim, E. S. Ruthazer, Microglial trogocytosis and the complement system regulate axonal pruning in vivo. *elife* **10**, e62167 (2021).
78. M. E. Price, B. A. McCool, Chronic alcohol dysregulates glutamatergic function in the basolateral amygdala in a projection-and sex-specific manner. *Front. Cell Neurosci.* **16**, 857550 (2022).
79. S. Zhao, A. D. Umpierre, L. J. Wu, Tuning neural circuits and behaviors by microglia in the adult brain. *Trends Neurosci.* **47**, 181–194 (2024).
80. M. A. S. Khan, S. L. Chang, Alcohol and the brain-gut axis: The involvement of microglia and enteric glia in the process of neuro-enteric inflammation. *Cells* **12**, 2475 (2023).
81. P. Mews, G. Egervari, R. Nativio, S. Sidoli, G. Donahue, S. I. Lombroso, D. C. Alexander, S. L. Riesche, E. A. Heller, E. J. Nestler, B. A. Garcia, S. L. Berger, Alcohol metabolism contributes to brain histone acetylation. *Nature* **574**, 717–721 (2019).
82. J. A. Pasman, K. J. H. Verweij, J. M. Vink, Systematic review of polygenic gene-environment interaction in tobacco, alcohol, and cannabis use. *Behav. Genet.* **49**, 349–365 (2019).
83. K. G. Chartier, K. J. Karriker-Jaffe, C. R. Cummings, K. S. Kendler, Review: Environmental influences on alcohol use: Informing research on the joint effects of genes and the environment in diverse U.S. populations. *Am. J. Addict* **26**, 446–460 (2017).
84. *Diagnostic and statistical manual of mental disorders: DSM-5™* (American Psychiatric Publishing Inc., ed. 5, 2013), pp. 947.
85. M. Jin, R. Xu, L. Wang, M. M. Alam, Z. Ma, S. Zhu, A. C. Martini, A. Jadali, M. Bernabucci, P. Xie, K. Y. Kwan, Z. P. Pang, E. Head, Y. Liu, R. P. Hart, P. Jiang, Type-I-interferon signaling drives microglial dysfunction and senescence in human iPSC models of Down syndrome and Alzheimer's disease. *Cell Stem Cell* **29**, 1135–1153.e8 (2022).
86. A. Maximov, Z. P. Pang, D. G. Tervo, T. C. Südhof, Monitoring synaptic transmission in primary neuronal cultures using local extracellular stimulation. *J. Neurosci. Methods* **161**, 75–87 (2007).
87. E. N. Oni, A. Halikere, G. Li, A. J. Toro-Ramos, M. R. Swerdel, J. L. Verpeut, J. C. Moore, N. T. Bello, L. J. Bierut, A. Goate, J. A. Tischfield, Z. P. Pang, R. P. Hart, Increased nicotine response in iPSC-derived human neurons carrying the CHRNA5 N398 allele. *Sci. Rep.* **6**, 34341 (2016).
88. L. Wang, V. R. Mirabella, R. Dai, X. Su, R. Xu, A. Jadali, M. Bernabucci, I. Singh, Y. Chen, J. Tian, P. Jiang, K. Y. Kwan, C. Pak, C. Liu, D. Comoletti, R. P. Hart, C. Chen, T. C. Südhof, Z. P. Pang, Analyses of the autism-associated neuroligin-3 R451C mutation in human neurons reveal a gain-of-function synaptic mechanism. *Mol. Psychiatry* **29**, 1620–1635 (2022).
89. M. S. Scarnati, A. J. Boreland, M. Joel, R. P. Hart, Z. P. Pang, Differential sensitivity of human neurons carrying mu opioid receptor (MOR) N40D variants in response to ethanol. *Alcohol* **87**, 97–109 (2020).
90. Y. Guo, Y. Chen, S. Carreon, M. Qiang, Chronic intermittent ethanol exposure and its removal induce a different miRNA expression pattern in primary cortical neuronal cultures. *Alcohol Clin. Exp. Res.* **36**, 1058–1066 (2012).
91. R. Lieberman, E. S. Levine, H. R. Kranzler, C. Abreu, J. Covault, Pilot study of iPS-derived neural cells to examine biologic effects of alcohol on human neurons in vitro. *Alcohol Clin. Exp. Res.* **36**, 1678–1687 (2012).
92. M. S. Scarnati, A. J. Boreland, M. Joel, R. P. Hart, Z. P. Pang, Differential sensitivity of human neurons carrying μ opioid receptor (MOR) N40D variants in response to ethanol. *Alcohol* **87**, 97–109 (2020).
93. K. Young, H. Morrison, Quantifying microglia morphology from photomicrographs of immunohistochemistry prepared tissue using ImageJ. *J. Vis. Exp.* **136**, 57648 (2018).
94. A. Karperien, H. Ahammer, H. F. Jelinek, Quantitating the subtleties of microglial morphology with fractal analysis. *Front. Cell Neurosci.* **7**, 3 (2013).
95. M. D. M. Fernandez-Arjona, J. M. Grondona, P. Granados-Duran, P. Fernandez-Llebrez, M. D. Lopez-Avalos, Microglia morphological categorization in a rat model of neuroinflammation by hierarchical cluster and principal components analysis. *Front. Cell. Neurosci.* **11**, 235 (2017).
96. A. Mortazavi, B. A. Williams, K. McCue, L. Schaeffer, B. Wold, Mapping and quantifying mammalian transcriptomes by RNA-Seq. *Nat. Methods* **5**, 621–628 (2008).
97. A. Halikere, D. Popova, M. S. Scarnati, A. Hamod, M. R. Swerdel, J. C. Moore, J. A. Tischfield, R. P. Hart, Z. P. Pang, Addiction associated N40D mu-opioid receptor variant modulates synaptic function in human neurons. *Mol. Psychiatry* **25**, 1406–1419 (2020).
98. M. E. Ritchie, B. Phipson, D. Wu, Y. Hu, C. W. Law, W. Shi, G. K. Smyth, limma powers differential expression analyses for RNA-sequencing and microarray studies. *Nucleic Acids Res.* **43**, e47 (2015).
99. C. W. Law, Y. Chen, W. Shi, G. K. Smyth, voom: Precision weights unlock linear model analysis tools for RNA-seq read counts. *Genome Biol.* **15**, R29 (2014).
100. W. S. Cleveland, Robust locally weighted regression and smoothing scatterplots. *J. Am. Stat. Assoc.* **74**, 829–836 (1979).
101. G. Yu, L. G. Wang, Y. Han, Q. Y. He, clusterProfiler: An R package for comparing biological themes among gene clusters. *Omics* **16**, 284–287 (2012).
102. Y. Hao, S. Hao, E. Andersen-Nissen, W. M. Mauck III, S. Zheng, A. Butler, M. J. Lee, A. J. Wilk, C. Darby, M. Zager, P. Hoffman, M. Stoeckius, E. Papalexi, E. P. Mimitou, J. Jain, A. Srivastava, T. Stuart, L. M. Fleming, B. Yeung, A. J. Rogers, J. M. McElrath, C. A. Blish, R. Gottardo, P. Smibert, R. Satija, Integrated analysis of multimodal single-cell data. *Cell* **184**, 3573–3587.e29 (2021).

Acknowledgments: We thank P. Jiang and M. Jin for supporting this research in guiding for microglial cell differentiation from iPSCs. The Child Health Institute of New Jersey is supported in part by the Robert Wood Johnson Foundation (RWJF grant #74260). We also thank other members of the Pang laboratory and the COGA consortium for the support and valuable comments. The COGA, Principal Investigators (PIs) B. Porjesz, V. Hesselbrock, and T. Foroud; Scientific Director, A. Agrawal; and Translational Director, D. Dick, includes 10 different centers: University of Connecticut (V. Hesselbrock); Indiana University (H.J. Edenberg, T. Foroud, Y. Liu, and M.H. Plawecki); University of Iowa Carver College of Medicine (S. Kuperman and J. Kramer); SUNY Downstate Health Sciences University (B. Porjesz, J. Meyers, C. Kamarajan, and A. Pandey); Washington University in St. Louis (L. Bierut, J. Rice, K. Bucholz, and A. Agrawal); University of California at San Diego (M. Schuckit); Rutgers University (J. Tischfield, D. Dick, R. Hart, and J. Salvatore); The Children's Hospital of Philadelphia, University of Pennsylvania (L. Almasy); Icahn School of Medicine at Mount Sinai (A. Goate and P. Slesinger); and Howard University (D. Scott). Other COGA collaborators include: L. Bauer (University of Connecticut); J. Nurnberger Jr., L. Wetherill, X., Xuei, D. Lai, and S. O'Connor, (Indiana University); G. Chan (University of Iowa; University of Connecticut); D.B. Chorlian, J. Zhang, P. Barr, S. Kinreich, and G. Pandey (SUNY Downstate); N. Mullins (Icahn School of Medicine at Mount Sinai); A. Anokhin, S. Hartz, E. Johnson, V. McCutcheon, and S. Saccone (Washington University); J. Moore, F. Aliev, Z. Pang, and S. Kuo (Rutgers University); A. Merikangas (The Children's Hospital of Philadelphia and University of Pennsylvania); H. Chin and A. Parsian are the NIAAA Staff Collaborators. We continue to be inspired by our memories of H. Begleiter and T. Reich, founding PI and co-PI of COGA, and also owe a debt of gratitude to other past organizers of COGA, including T.-K. Li, P. Michael Conneally, R. Crowe, and W. Reich, for the critical contributions. **Funding:** This study was supported by the NIAAA grant R01AA023797 (to Z.P.P.) and COGA U10AA008401 (R.P.H.). A.J.B. was supported by NIGMS NIH T32GM008339 and by NCATS NIH TL1TR003019. **Author contributions:** Conceptualization: Z.P.P., R.P.H., X.L., P.A.S., J.L.M., J.T., X.L., J.S., P.B.B., D.D., J.D., R.P.H., A.J.B., and H.J.E. Methodology: X.L., Z.P.P., R.P.H., P.A.S., J.L.M., J.T., P.B.B., A.J.B., J.L., S.K., and A.K. Software: J.L., J.L.M., P.B.B., S.Z., and R.P.H. Validation: J.L.M., X.L., A.J.B., A.C.S., Z.P.P., and S.K. Formal analysis: X.L., J.L., P.B.B., S.Z., R.P.H., A.K., Z.P.P., Y.A., and S.K. Investigation: L.C., X.L., J.L., A.J.B., S.K., H.J.E., R.P.H., and Z.P.P. Resources: J.T., J.S., P.B.B., R.P.H., Z.P.P., H.J.E., A.A., Y.L., and D.D. Data curation: X.L., R.P.H., W.K., J.L., and Z.P.P. Writing—original draft: X.L., Z.P.P., R.P.H., P.A.S., J.L., A.K., S.K., and J.L.M. Writing—review and editing: X.L., J.L., A.J.B., D.L., J.L.M., C.K., J.T., J.S., P.B.B., W.K., A.J.B., S.K., P.A.S., J.D., D.D., R.P.H., H.J.E., A.A, Y.L., and Z.P.P. Visualization: X.L., J.L., J.L.M., S.Z., A.C.S., H.J.E., R.P.H., and Z.P.P. Supervision: R.P.H., Z.P.P., and A.K. Project administration: Z.P.P. Funding acquisition: Z.P.P., J.L.M., J.T., J.S., R.P.H., Z.P.P., and H.J.E. **Competing interests:** D.D. is a cofounder of Thrive Genetics Inc. and a member of the advisory board of Seek Health Group Inc. She owns stock in both companies. The other authors declare that they have no competing interests. **Data and materials availability:** RNA-seq data are available on the Gene Expression Omnibus (GEO): GSE255988 for microglial cell mRNA sequencing and GSE271585 for iPSC mRNA sequencing. The source code for data processing and analysis for this study has been deposited on Zenodo (https://zenodo.org/doi/10.5281/zenodo.12773329). All data needed to evaluate the conclusions in the paper are present in the paper and/or the Supplementary Materials.

Submitted 15 February 2024
Accepted 4 October 2024
Published 8 November 2024
10.1126/sciadv.ado5820